

# Point defect engineering in thin-film solar cells

Ji-Sang Park<sup>1</sup>, Sunghyun Kim<sup>1</sup>, Zijuan Xie<sup>1,2</sup>, and Aron Walsh<sup>1,3\*</sup>

<sup>1</sup>Thomas Young Centre and Department of Materials, Imperial College London, London SW7 2AZ, UK

<sup>2</sup>Department of Physics, Harbin Institute of Technology, 92 Xidazhi Street, Harbin 150001, China

<sup>3</sup>Department of Materials Science and Engineering, Yonsei University, Seoul 03722, Korea

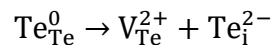
\*e-mail: [a.walsh@imperial.ac.uk](mailto:a.walsh@imperial.ac.uk)

**Control of defect processes in photovoltaic materials is essential for realising high-efficiency solar cells and related optoelectronic devices. The concentrations of native defects and extrinsic dopants tune the Fermi level and enable semiconducting p-n junctions; however, fundamental limits to doping exist in many compounds. Optical transitions involving defect states can enhance photocurrent generation through sub-bandgap absorption; however, such states are often responsible for carrier trapping and non-radiative recombination events that limit open-circuit voltage. Many classes of materials – including metal oxides, chalcogenides, and halides – are being examined for next-generation solar energy applications, and each technology faces distinct challenges that could benefit from point defect engineering. We review the evolution in point defect behaviour from Si-based photovoltaics to thin-film CdTe and Cu(In,Ga)Se<sub>2</sub> technologies, through to the latest generation halide perovskite (CH<sub>3</sub>NH<sub>3</sub>PbI<sub>3</sub>) and kesterite (Cu<sub>2</sub>ZnSnS<sub>4</sub>) devices. We focus on the chemical bonding that underpins the defect chemistry, and the atomistic processes associated with the photophysics of charge carrier generation, trapping, and recombination in solar cells. Finally, we outline general principles to enable defect control in complex semiconducting materials.**

An understanding of defects and defect processes is necessary to enable functionality and control efficiency in semiconductor devices<sup>1,2</sup>. For applications in light conversion – including solar cells and solar fuels – photo-generated electrons and holes must have lifetimes sufficient for collection or reaction before recombination occurs. On one hand, defects in semiconducting materials can limit the transport (mobility and diffusion lengths) of charge carriers, while on the other hand they are important for tuning the carrier concentrations and Fermi level for realising p-type (hole conducting) and n-type (electron conducting) materials. The formation of defects that introduce levels deep ( $\gg k_B T$ ) in the bandgap of a photovoltaic semiconductor should generally be avoided. Such levels can be formed intrinsically or extrinsically and can trap electrons or holes, resulting in lower carrier extraction efficiency. Each photovoltaic technology shares the same fundamental principle of light-to-electricity conversion, but can feature distinct defect processes (see Table 1). Here, we review the defect chemistry and physics of a range of photovoltaic materials from an elemental semiconductor to multi-component compound semiconductors and hybrid organic-inorganic compounds. We link the underlying crystal structures and chemical bonding to trends in defect formation energy and concentrations, optical levels, and electron-hole recombination rates. We show how the requirements for defect tolerance and control have evolved from Si to thin-film CdTe and Cu(In,Ga)(S,Se)<sub>2</sub> (CIGS) technologies, through to the latest generation of perovskite and kesterite solar cells.

### Classification of point defects

The statistical mechanics of defects in crystalline materials has been studied for almost a century. The atoms in crystalline materials form a regular lattice, but it was realised by Frenkel<sup>3</sup> that in thermal equilibrium a number of atoms will leave their regular sites. Starting from a perfect crystal, such a process creates two point defects: an interstitial defect and the associated atomic vacancy, which may be in neutral or charged states. Taking the example of CdTe and using the standard notation  $Species_{Lattice\ site}^{Relative\ charge}$ , the formation of a charged tellurium Frenkel pair ( $V_{Te}^{2+} + Te_i^{2-}$ ) can be written as:



where the reactants (left-hand side) represent two atomic sites in the perfect crystal, and the product (right-hand side) contains a charged vacancy and interstitial involving the Te anion. Site vacancies

and interstitials are two of the most common point defects, in addition to antisites such as the  $[\text{Cu}_{\text{Zn}}^- + \text{Zn}_{\text{Cu}}^+]$  complex common in  $\text{Cu}_2\text{ZnSnS}_4$ . Using the notation developed by Kröger and Vink, the relative effective charges are given using dots (positive), dashes (negative) and crosses (neutral)<sup>4</sup>, e.g.  $V_{\text{Te}}^{2+} \equiv V_{\text{Te}}^{\cdot\cdot}$ .

The concentration of a given point defect in a material at equilibrium is determined by its free energy of formation (see Box 1), which in turn depends on the chemical potentials of the system including the growth environment (atomic chemical potentials) and the Fermi level (electronic chemical potential). The atomic chemical potentials can be controlled, for example, using the temperature and partial pressure of sulphur vapours in the chamber for the synthesis of CIGS thin films.

The enthalpic cost of point defect formation typically falls in the range 0–10 eV, with concentrations ranging from  $10^{15}$ – $10^{20}$   $\text{cm}^{-3}$ , with the high end of the range corresponding to an imperfection of around 1 in every 100 lattice sites. The defect formation energy can become negative in the case of materials that favour non-stoichiometry such as copper telluride ( $\text{Cu}_{2-x}\text{Te}$ ), which is used as a back electrical contact in some CdTe device architectures. There is a well-developed theoretical framework for calculating the energetics of defect formation, which has evolved from classical simulations<sup>5</sup> to modern first-principles techniques including those based on density functional theory (DFT)<sup>6</sup>. A given point defect can exist in a variety of charge states, and may transition between them by exchanging electrons or holes with the valence or conduction bands of the semiconductor host. A classification of the various defect levels in semiconductors is given in Box 2.

Point defects are not necessarily static in the lattice, but diffuse with a rate that is limited by the activation energy for solid-state diffusion. Ion transport can proceed according to a variety of mechanisms that includes vacancy and interstitial-mediated diffusion. The self-diffusion coefficient of Si is  $\sim 10^{-16}$   $\text{cm}^2/\text{sec}$  (1000 °C, slow process),<sup>7</sup> while Cd diffuses at  $\sim 10^{-9}$   $\text{cm}^2/\text{sec}$  in CdTe (1000 °C),<sup>8</sup> Cu diffuses up to  $10^{-8}$   $\text{cm}^2/\text{sec}$  in  $\text{CuInSe}_2$ ,<sup>8</sup> and  $> 10^{-5}$   $\text{cm}^2/\text{sec}$  in Si (380 °C, fast process)<sup>9</sup>. In a working solar cell, built-in electric fields can further enhance the diffusion rates (ion drift and electromigration), and in severe cases can give rise to hysteresis – a dependence of the history of the device – in the current-voltage response<sup>10</sup>.

The identification of point defects in materials is challenging owing to their dilute concentrations, which are beyond the resolution of most standard materials characterisation techniques (e.g. X-ray diffraction). The assignment of particular signals often requires a multi-technique approach with experimental analysis assisted by theory and simulation. Point defects can be probed optically (e.g. photoluminescence and photoconductivity), thermally (e.g. deep-level transient spectroscopy and thermally-stimulated conductivity), vibrationally (e.g. through infra-red and Raman spectroscopy), and magnetically (e.g. electron-spin resonance). Even in well-studied optoelectronic materials including ZnO and GaN, the atomic origin of specific defect luminescence features remains the subject of on-going research and debate<sup>11</sup>. Sub-bandgap defect levels reported in a range of photovoltaic materials are summarised in Table 2, showing that the defect levels are widely distributed within the bandgap. As discussed below for each technology, innovative procedures have been developed for avoiding the most detrimental of these defects in order to realise efficient light-to-electricity conversion in operating solar cells.

## **Silicon**

Silicon is one of the most abundant chemical elements. It naturally forms a face-centred-cubic diamond structure (space group  $Fd3m$ , see Figure 1a) with tetrahedral local coordination environments around each atom. Crystalline Si has a strongly indirect bandgap of 1.12 eV at 300 K with lighter hole ( $0.15 m_e$ ) than electron ( $0.19 m_e$ ) effective masses<sup>12</sup>. The associated relative dielectric constant is approximately 12 at room temperature<sup>12</sup>. In tetrahedral elemental semiconductors, it is common to describe the bonding in terms of the overlap of s and p atomic orbitals forming  $sp^3$  hybrid orbitals, with the valence band composed of bonding combinations, and the conduction band consisting of the corresponding antibonding combinations.

Si solar cells represent a mature photovoltaic technology<sup>13,14</sup>, and thus many aspects of point defects have been thoroughly investigated and documented over the past 60 years. In this section, we introduce some essential features of defect engineering in Si photovoltaics, which can be potentially transferred to emerging photovoltaic technologies. For a more comprehensive overview of defect processes in Si, a number of good reviews are available<sup>15,16</sup>.

*Doping efficiency* of a potential photovoltaic material is critical as some photovoltaic cell architectures require both n-type and p-type semiconductors to form a p-n or p-i-n junction. Si has ideal impurities in the form of boron (electron acceptor) and phosphorous (electron donor), which

are shallow dopants for p-type and n-type behaviour, respectively. Thus homo-junction p-n Si solar cells are readily achieved. Both types of wafers are available; however, p-type wafers have been widely used as B has higher segregation coefficient than P, making it advantageous to obtain a spatially homogeneous doping profile<sup>14</sup>. Diffusivity and diffusion mechanisms of dopants have been thoroughly analysed as the front n-type or p-type regions are made by phosphorous and boron diffusion, respectively<sup>16</sup>.

*Recombination rates* must be controlled to achieve long lifetime of electrons and holes to extract photo-generated carriers. A range of recombination processes for photo-generated electrons and holes are summarised in Box 3. The challenge for Si has been the suppression of non-radiative losses including defect-induced deep-level (Shockley-Read-Hall, SRH) and surface recombination pathways<sup>17–19</sup>. Radiative and Auger recombination coefficients are intrinsic properties of a material, leaving less room for improvement. While Auger recombination only becomes significant at high injection levels (light intensity) for direct bandgap materials, due to the strongly indirect bandgap of Si (low radiative recombination rate), Auger processes limit the theoretical maximum device efficiency to around 29% under 1-sun illumination<sup>20</sup>.

Careful control of surface passivation has been necessary in Si solar cells to realise practical large-area high-efficiency devices<sup>18,19</sup>. From an atomistic perspective, low-coordinated Si atoms at the Si surface have amphoteric dangling bonds that introduce a half-occupied deep level in the bandgap<sup>21,22</sup>. These deep levels can be chemically passivated by hydrogen atoms<sup>23</sup>, which can be supplied from a hydrogenated silicon nitride layer<sup>14,19</sup> or amorphous Si<sup>13</sup>. Further migration of H into bulk region can neutralise shallow dopants; interstitial H acts as a donor and acceptor in p-type and n-type Si, respectively<sup>24</sup>. Besides hydrogen passivation, surface electron-hole recombination also can be reduced by using a fixed charge in the dielectric layer, which repels one type of carrier and attract the other<sup>14,25</sup>, reducing the rate of SRH recombination<sup>19</sup>.

*Impurity control* is essential in Si as many common unintentional metal impurities are detrimental to the photovoltaic efficiency<sup>15,26–28</sup>. The thermal stability of impurities and their electrical properties have been thoroughly documented<sup>29–31</sup>. Low-cost solar-grade Si wafers generally have higher concentration of recombination centres (metal concentration < 200 ppbw) as compared to electronics-grade Si (< 2 ppbw)<sup>32–35</sup>. The solubility and diffusivity of transition metals measured by several techniques shows an increasing trend from Ti to Cu<sup>27,28,36,37</sup>. Defect levels of metal

impurities have been investigated by both spectroscopic methods<sup>26,28,36,38–42</sup> and quantum mechanical simulations<sup>43,44</sup>. The most detrimental impurities can be removed from the material using various processing techniques (e.g. gettering and control of precipitates)<sup>32,37,45,46</sup>.

Given the long history of Si research, the understanding and assignment of defects has evolved over time. Re-evaluation of defect processes using state-of-the-art techniques can challenge accepted understanding, for example, as shown in the study of Ni diffusivity in Si where estimates of the solid-state diffusion barrier decreased from 0.47 eV to 0.15 eV<sup>47</sup>. From a theoretical perspective, most initial simulations of defects processes in Si relied on approximate methods. The first wave of DFT calculations based on the local density approximation (LDA) suffered from large errors in structure and bandgaps, which required *a posteriori* correction schemes. The fundamental properties of point and complex defects are being revisited using advanced methods – including hybrid DFT functionals that incorporate a fraction of exact Hartree-Fock exchange to address electron self-interaction, and many-body *GW* theory to include quasi-particle excitations – to remove bandgap underestimation and thus allow the calculated defect levels to be directly compared to measured values<sup>44,48</sup>. Recent studies have further shown that migration barriers in Si can be predicted with smaller errors using recently developed DFT exchange-correlation functionals<sup>44,49,50</sup>.

*Device aging and lifetime* effects in solar cells often involve the role of chemical impurities and point defect processes over longer timescales, in particular for light-induced degradation (LID) and potential-induced degradation (PID). Control of the defects responsible for device degradation is of key importance for Si-based technologies as they have already achieved high-efficiency in large-area devices<sup>51</sup>. A well-documented mechanism is boron-oxygen LID, which is mainly observed in B-doped Czochralski (cz) grown Si<sup>52–54</sup>. Typical cz-Si samples contain oxygen impurities of around  $10^{18} \text{ cm}^{-3}$ , much higher as compared to float-zone Si as quartz crucibles are used in the manufacture. Various models have been suggested and examined to explain the degradation phenomena; however, there is no consensus on the atomistic process<sup>52–54</sup>. Substitution of Ga for B is found to be beneficial, but Ga has a worse segregation coefficient in Si than B<sup>52</sup>. The degradation rate can be relieved by using  $\text{SiN}_x$  with low  $x$  or by substituting soda-lime glass with other glass compositions<sup>14</sup>. Many high-efficiency Si solar cells are now based on n-type Si<sup>55–57</sup>, which is free from this degradation pathway<sup>52</sup>.

Copper is responsible for another LID mechanism, and substitutional Cu and/or precipitated Cu clusters are suggested to be responsible for the degradation<sup>7</sup>. It can be removed by negative corona discharge on the wafer surfaces to attract positively charged Cu ions and subsequent etching of the Cu-rich surface layer<sup>58</sup>.

Sodium-contaminated stacking faults (SFs) has been linked to a PID of shunting type. Positively charged Na ions drift from soda-lime glass or surface of SiN<sub>x</sub> towards the SiN<sub>x</sub>/Si interface due to the electric field and Na contaminated SFs are formed under long-term device operation<sup>59</sup>. Contaminated SFs can serve as channels for charge carrier transport, resulting in reduced shunt resistance, which lowers the efficiency (open-circuit voltage and fill factor) of a solar cell. The degraded cells can be partially recovered by out-diffusion of Na driven by thermal energy or the application of a reverse-bias voltage<sup>59</sup>.

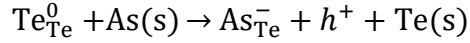
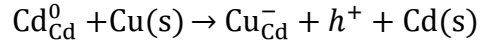
### **Cadmium telluride**

CdTe is a compound semiconductor that also adopts a face-centred cubic crystal structure (zincblende, space group  $F\bar{4}3m$ , see Figure 1c). The material has a bandgap of 1.48 eV at 300 K with electron and hole effective masses below 0.15  $m_e$ , making it ideal for single-junction solar cell applications<sup>12</sup>. The formal electronic configuration of Cd<sup>2+</sup> 4d<sup>10</sup>5s<sup>0</sup> and Te<sup>2-</sup> 5s<sup>2</sup>5p<sup>6</sup> suggest an upper valence band formed of Te 5p orbitals, and a lower conduction band formed of Cd 5s orbitals, as found in band structure calculations<sup>60</sup>. The polarity of the Cd-Te bond (optical phonon modes above 4 THz) results in a significant difference between the high-frequency relative dielectric constant of 7.1 and the low-frequency (or static) relative dielectric constant of 10.4.

CdTe solar cells have more fundamental problems than Si; in particular, related to low doping efficiency and high electron-hole recombination rates<sup>61-67</sup>. Currently, the best CdTe devices are based on a p-type CdTe/n-type CdS heterojunction, and one concern is whether a high enough hole concentration can be achieved in CdTe thin-films. The dominant intrinsic acceptor defect in CdTe is the Cd vacancy ( $V_{Cd}$ ), and the associated acceptor level is deep around 0.4 eV according to recent hybrid-DFT (HSE) calculations<sup>67-70</sup> (see Figure 2). Higher concentrations of the ionised Cd vacancy defect can be in principle achieved if CdTe is grown under Cd-poor and Te-rich conditions, and can be further enhanced if the layer is grown at high temperature and subsequently quenched<sup>71</sup>. The formation energy of defects with different charge states were used to estimate the net hole

concentration, which is limited to around  $10^{15} \text{ cm}^{-3}$  unless there are additional dopants present<sup>67</sup>. Extrinsic p-type dopants are necessary to enhance the hole concentration of CdTe.

Obvious candidates for p-type doping are Group 1 or Group 11 elements substituting for Cd, and Group 15 elements substituting  $\text{Te}^{72,73}$ , for example:



Experimentally, Cu has been used as an acceptor dopant in the material<sup>74</sup>. The formation energy of  $\text{Cu}_{\text{Cd}}$  defect is sufficiently low (for high solubility), and its acceptor level is found to be shallower than that of  $\text{V}_{\text{Cd}}$  (for efficient ionisation)<sup>67,70</sup>. Cu impurities can be incorporated in the form of interstitials, which are electron donors; however, their relative concentration can be modulated by controlling the atomic chemical potentials<sup>67</sup>. However,  $\text{Cu}_{\text{Cd}}$  defects can capture a significant amount of minority electron carriers as the Cu concentration increases (capture cross section  $\sim 10^{-16} \text{ cm}^{-2}$ )<sup>75-77</sup>. Therefore, the concentration and doping profile should be carefully controlled<sup>62</sup> through knowledge of their diffusion mechanism and pathways<sup>78</sup>. On the other hand, doping of group 15 elements (P and As) has been attempted experimentally<sup>65</sup> as they can introduce shallow acceptor levels when coordinated tetrahedrally<sup>67,79</sup>.

It has been predicted that  $\text{P}_{\text{Te}}$  and  $\text{As}_{\text{Te}}$  can be converted to a deep donor that acts to limit the doping efficiency, which is termed an AX centre<sup>67,79</sup>. AX centres involve breaking of two nearest-neighbour bonds and forming a new bond between the impurity and a neighbouring Te atom. The AX centre is thus formed when the electronic energy gain is higher than the energy cost to break the bonds<sup>67,79</sup>. The self-compensation can be partly overcome by non-equilibrium growth; a hole density as high as  $10^{17} \text{ cm}^{-3}$  was predicted to be achievable under certain conditions<sup>67,79</sup>. Group 1 elements have the potential to enhance hole concentrations when CdTe is grown under Te-rich conditions owing to the increased stability of the substitutional form as compared to interstitials<sup>67</sup>.

Doping efficiency is one problem, and short minority carrier lifetime is another in CdTe solar cells. Photo-generated electron and hole lifetime is an important material parameter to achieve high-efficiency devices. Time-resolved photoluminescence (TRPL) measurements have shown that the open-circuit voltage ( $V_{\text{oc}}$ ) generally increases with lifetime in CdTe devices<sup>76</sup>. DFT calculations (generalised-gradient approximation with the PBE functional) suggested that the Te vacancy acts



as the major recombination centre<sup>63,80</sup>, whose formation can be suppressed when the CdTe absorber layer is grown under Te-rich conditions. However, carrier lifetime measured by two-photon excitation TRPL measurements is longer in CdTe grown under Cd-rich conditions<sup>61</sup>. Bulk recombination can be more accurately captured by two-photon excitation (2PE) than one-photon excitation (1PE) as 1PE TRPL is sensitive to surface recombination<sup>61,76,81</sup>. Hybrid-DFT (HSE) calculations helped to resolve this contradiction as  $V_{Te}$  is confirmed to be a shallow defect and Te antisite defect ( $Te_{Cd}$ ) becomes the deep-level recombination centre to be avoided<sup>61,67</sup>. This series of studies again emphasises that defects should be examined by computational methods that are free from large bandgap and delocalisation errors. Deep levels in CdTe are well documented experimentally<sup>82-87</sup>; however, the atomistic origins of many defects remain unassigned and the measured values vary considerably<sup>84</sup>.

If electron-hole recombination is sufficiently reduced in the bulk material, then recombination at extended defects (grain boundaries (GBs), surfaces, and interfaces) becomes essential to improve the performance of CdTe solar cells<sup>66,88</sup>. It has been shown that Te-rich surfaces exhibit higher surface recombination velocity than stoichiometric or Cd-rich surfaces. Dangling bonds and/or dimerised octet-rule-violating (Te-Te) bonds were suspected to be origin of faster surface recombination<sup>64</sup>, which are also formed at extended defects<sup>67,89,90</sup>. In polycrystalline semiconductors, GBs are generally harmful to the device efficiency because of fast non-radiative recombination;<sup>91</sup> however, polycrystalline CdTe solar cells exhibit *higher* solar conversion efficiencies than monocrystalline CdTe solar cells<sup>89,92-94</sup>. GBs can exist in a wide variety of forms, but certain configurations are lower in energy to form<sup>95</sup>. Theoretical studies suggest that deep levels formed at GBs act as recombination centers,<sup>95,96</sup> showing an atomistic similarity to the Te-on-Cd antisite point defect<sup>61,97</sup>.

Chloride treatment, especially  $CdCl_2$ , has been widely used to activate CdTe, but the microscopic processes are still in debate with a number of proposed models<sup>98-100</sup>.  $CdCl_2$  treatment improves carrier lifetime<sup>81,91,101,102</sup>, which could originate from the passivation of interface states<sup>74,103</sup> and/or GBs<sup>90,96</sup>, band bending at GBs<sup>89,92</sup>, elimination of deep levels<sup>85,104</sup>, and removal of stacking faults<sup>100,105</sup>. Recently Barnard *et al.* reported that the chloride treatment reduces surface, interface, and GB recombination using three-dimensional 2PE-TRPL microscopy<sup>81</sup>. Consistent with these findings, large-grain polycrystalline CdTe without the  $CdCl_2$  treatment was found to have long carrier lifetime<sup>102</sup>, while  $CdCl_2$  treatment increases the grain size<sup>94,99</sup>. Origin of the increased

lifetime at the GBs could be due to band bending at GBs<sup>89,92</sup> or passivation of GBs by impurity segregation<sup>96</sup>. In one model, Cl ions segregate to the GBs and form Cl<sub>Te</sub> defects, which donate one electron either to the conduction band (free carriers) or deep gap states (trapped carriers) and become positively charged<sup>89</sup>. Such positively charged ions bend bands, forming local p-n junctions, and thus charge separation is enhanced.

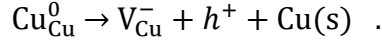
Certain extended defects can be passivated by Cu and Cl impurity incorporation<sup>96</sup>. On the other hand, sulfur incorporation could be also responsible for the less detrimental GBs. Increase of the lifetime is higher near the CdTe/CdS junction<sup>81</sup>, where the S concentration is higher because of inter-diffusion<sup>106–108</sup>. It was shown that sulphur atoms mostly reside at the GBs<sup>101</sup>, and that can result in less detrimental GB as S-Te or S-S octet-rule-violating bonds induce a shallower anti-bonding level than Te-Te bonds<sup>90</sup>. MgCl<sub>2</sub> treatment was also suggested for the aims of reducing the cost and increasing the environmental benefit<sup>109</sup>, whereas CdCl<sub>2</sub> is advantageous to incorporate Cl more easily because of a smaller bond dissociation energy<sup>108</sup>.

## Chalcopyrites

Following the single component (Si) and dual component (CdTe) materials, CuInSe<sub>2</sub> (CIS) is a ternary semiconductor that also adopts a diamond-related crystal structure (see Figure 1e). The chalcopyrite mineral structure features roughly tetrahedral coordination environments, but the tetragonal lattice (space group  $I\bar{4}2d$ ) allows for additional internal distortions of the Se atoms (crystal field splitting). The formal electronic configuration of Cu<sup>+</sup> 3d<sup>10</sup>4s<sup>0</sup>, In<sup>3+</sup> 5s<sup>0</sup>5p<sup>0</sup> and Se<sup>2-</sup> 4s<sup>2</sup>4p<sup>6</sup> suggests an upper valence band formed of Cu 3d and Se 4p orbitals, and a lower conduction band formed of In 5s and Cu 4s orbitals, as found in early band structure calculations<sup>110</sup>. The material has a bandgap of 1.01 eV at 300 K, but often the Cu(In,Ga)(S,Se)<sub>2</sub> (CIGS) solid-solution is used to tune the optical response: chemical substitution of In by Ga (and Se by S) widens the bandgap. The relative dielectric constants of CuInSe<sub>2</sub> are 8.5 (9.5  $\epsilon_c$ ) for high-frequency and 15.2 (16.0  $\epsilon_c$ ) for the static limit are approximately 20% larger than those of Si and CdTe<sup>12</sup>.

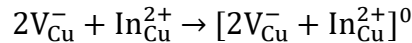
CIGS represents another promising thin-film solar cell technology, which is currently available on the market<sup>111</sup>. Photovoltaic conversion efficiency exceeding 20% has been achieved by careful defect process engineering. As a multi-component system, the defect processes in CIGS are more complicated than for Si or CdTe, and direct assignment of electronic and optical signatures to specific point defects becomes even more difficult.

Firstly, CIGS thin-films are *self-doped* p-type by intrinsic defects, without extrinsic impurities such as B and P employed in Si. The Cu vacancy ( $V_{Cu}$ ) is responsible for p-type doping, whose acceptor level is shallow and formation energy is low<sup>112–115</sup>.



Recent calculations<sup>116,117</sup> highlighted that Cu antisites ( $Cu_{In}$  and  $Cu_{Ga}$ ) may also substantially contribute to p-type doping. While  $Cu_{(In,Ga)}$  is predicted to be a deeper acceptor than  $V_{Cu}$ ,  $Cu_{(In,Ga)}$  is expected to be more abundant for materials processed under Cu-rich conditions.

Isolated  $In_{Cu}$  and  $Ga_{Cu}$  antisite defects have deep donor levels in the bandgap, which can trap minority carriers (electrons)<sup>113,114</sup>. However, experiments<sup>118,119</sup> revealed that CIGS exhibits excellent electronic properties even for heavy off-stoichiometry. Defect-defect interactions are largely responsible for the defect tolerance of CIGS, with several models proposed. The formation of defect complexes involving  $In_{Cu}$  and  $V_{Cu}$  has been predicted to remove deep levels in the bandgap<sup>113,114</sup>. The high binding energy indicates that  $V_{Cu}$  tends to form aggregates with antisite defects, turning the deep donors into electrically benign defect complexes, for example:



Under grossly off-stoichiometric conditions, defect complexes give rise to the formation of n-type ordered defect compounds (ODC) at the near surface region<sup>113,114</sup>. The CIGS/ODC interface forms a high-quality *p-n* heterojunction<sup>120</sup>. The good lattice match between CIGS and off-stoichiometric ODC prevents carrier trap forming at the interface. The electronic band alignment does not produce an electron barrier and serves to maximise the open-circuit voltage. Thus, the favourable optoelectronic properties of non-stoichiometric CIGS can be attributed to the formation of ODC. On the other hand, a recent hybrid-DFT study<sup>117</sup> argued that the binding energy of  $[2V_{Cu}^- + In_{Cu}^{2+}]$  is not large enough to be responsible for this effect; their calculated binding energy of 0.3 eV is smaller than previous reports. Instead, they suggest that it is a shallow donor level of  $In_{Cu}$  that results in the defect tolerance of CIGS. More quantitative models beyond the dilute defect limit, including a description of the complexation kinetics (e.g. using Monte Carlo techniques) are needed on this topic.

Defect complexes are also responsible for light-induced and voltage-bias-induced metastability in CIGS. The  $V_{OC}$  and capacitance of CIGS increases under illumination with *long-wavelength*

light<sup>121–123</sup>. The application of a reverse-bias voltage leads to a similar effect<sup>124,125</sup>. These changes are explained by a metastable increase of net acceptor concentration. On the other hand, the *short-wavelength* illumination leads to the opposite effect of a decreased net acceptor density<sup>126</sup>. Lany and Zunger<sup>127</sup> proposed that a (partial Schottky) defect complex of  $V_{Se}-V_{Cu}$  is the origin of the light- and bias-induced metastability. The  $V_{Se}-V_{Cu}$  complex exhibits amphoteric behaviour, acting as either a donor or acceptor depending on the position of the Fermi level in the bandgap. Persistent electron (hole) capture converts the  $V_{Se}-V_{Cu}$  complex from a shallow donor (acceptor) into a shallow acceptor (donor), accompanying the metastable change in atomic configuration.

Antisite defects, such as  $Ga_{Cu}$  in CIGS, are also pointed out as the metastable defects that limit  $V_{oc}$ . In III-V and II-VI semiconductors, such as GaAs and ZnSe, certain extrinsic donors, called DX centres, capture electrons, rather than donating them, accompanying large bond-breaking relaxation<sup>128–130</sup>. In CIGS, intrinsic DX-like behaviour is associated with  $Ga_{Cu}$  capturing an electron<sup>131</sup>. The optical absorption facilitates carrier capture and recombination with structure relaxation. The electron trap and non-radiative recombination due to a DX centre is responsible for the drop of photovoltaic energy conversion efficiency, which is more significant in Ga-rich CIGS.

Increased p-type conductivity has been observed in CIGS containing alkali metals such as Na and K<sup>132–135</sup>. The origin for the increased p-type conductivity is attributed to a variety of point defects and the passivation of grain boundaries. Based on DFT calculations<sup>136</sup>, Forest *et al* proposed that Na incorporation decreases the formation of  $In_{Cu}$  antisites, by forming  $Na_{Cu}$ , and thereby enhancing the hole concentration. On the other hand, Na antisites,  $Na_{(In,Ga)}$ , can act as electron acceptors<sup>132</sup>. However, they are not likely to contribute to the increased hole concentration due to their high formation energies<sup>136–138</sup>. Na and K also tend to segregate to the grain boundaries and passivate donor defects<sup>139,140</sup>.

Similar to CdTe solar cells, a lot of attention been devoted to the understanding of grain boundaries in CIGS<sup>141–145</sup>. Studies suggest that Cu-deficient GBs act as hole barriers as the valence band edge energy is lowered<sup>141,145</sup> and that deep levels of octet-rule violating bonds in GBs can be passivated by segregation of defects<sup>144</sup>. Band bending can occur because of the segregated charged defects in the GBs which modifies the long-range electrostatic potential<sup>142</sup>. Anti-correlation of the Cu and In composition ratio in the GBs has also been measured<sup>143</sup>.

## Kesterites

I<sub>2</sub>-II-IV-VI<sub>4</sub> quaternary semiconductors are a natural extension of II-VI (zincblende) and I-II-VI<sub>2</sub> (chalcopyrites) to more complex compounds, as explored in early work of Goodman<sup>146</sup> and Pamplin<sup>147,148</sup>, and later using DFT-based screening procedures<sup>71,149,150</sup>. The crystal structure adopted by many of these compounds is based on the kesterite mineral (space group  $I\bar{4}$ ), with a specific arrangement of the I, II and IV cations on a diamond lattice, with spontaneous ordering in (201) planes that can be related back to the chalcopyrite structure<sup>149</sup>. Kesterites share many similarities to chalcopyrites in terms of chemical bonding, physical properties and photovoltaic device architectures. The principal advantage is the replacement of In and Ga by the more sustainable (lower cost and increased abundance) elements Zn and Sn. The bandgap of Cu<sub>2</sub>ZnSnS<sub>4</sub> (CZTS) is around 1.5 eV at room temperature, which can be lowered to 1.0 eV by alloying with Se towards Cu<sub>2</sub>ZnSnSe<sub>4</sub> (CZTSe)<sup>151</sup>.

The performance of kesterite solar cells is currently limited by a low open-circuit voltage<sup>152</sup>. The current record photovoltaic efficiency of 12.6%<sup>153</sup> for kesterite solar cells is still below commercially competitive levels (15–20%). The possible origins of the low performance and V<sub>oc</sub> deficit are bandgap fluctuations reducing the effective bandgap, poor electrical contacts between CZTS and the Mo (back) or CdS (front) buffer layer resulting in rapid electron-hole recombination, and deep-level defects acting as non-radiative recombination centres in the bulk material<sup>154</sup>.

Defect formation in quaternary compounds like CZTS is highly sensitive to the chemical potentials (growth conditions) with four elements (three cations) to control<sup>155–159</sup> (see Figure 3). The existence of secondary phases such as ZnS and Cu<sub>2</sub>SnS<sub>3</sub> (CTS) limits the choice of growth conditions to avoid harmful defects such as deep donors. The chemical potentials need to be adjusted carefully to form phase-pure CZTS and not to form harmful secondary phases and defects, simultaneously. Under Cu-rich conditions, highly conductive Cu<sub>2</sub>S may be formed and electrically short the device. The Zn-rich phase ZnS has a wide bandgap, reducing the absorption and hindering current collection. Zn-poor conditions lead to the formation of CTS, which has a bandgap smaller than CZTS<sup>160</sup>. The volatile nature of Sn makes SnS<sub>2</sub> evaporate during the sulfurisation process, leaving the Sn-poor secondary compounds, such as Cu<sub>2</sub>S and ZnS. The remaining SnS<sub>2</sub> also may contribute to a high carrier recombination rate<sup>161</sup>. Due to the narrow phase stability field of CZTS and the existence of rich secondary phases and defects, it is difficult to achieve high-quality CZTS

crystals or films. The associated structural and electronic inhomogeneity results in poor device performance relative to the theoretical maximum light conversion efficiency.

In CZTS, there are two competing acceptors,  $\text{Cu}_{\text{Zn}}$  and  $\text{V}_{\text{Cu}}$ , which are formed in Cu-rich or Cu-poor conditions, respectively<sup>155,156,159</sup>. The acceptor level of  $\text{Cu}_{\text{Zn}}$  is deeper than that of  $\text{V}_{\text{Cu}}$ . However, the lower formation energy of  $\text{Cu}_{\text{Zn}}$  indicates its concentration is higher than that of  $\text{V}_{\text{Cu}}$ . Therefore, under Cu-rich conditions,  $\text{Cu}_{\text{Zn}}$  contributes to hole carrier concentrations more significantly, while  $\text{V}_{\text{Cu}}$  is responsible for the hole carriers under Cu-poor conditions. The abundance of  $\text{Cu}_{\text{Zn}}$  and  $\text{V}_{\text{Cu}}$  makes CZTS an intrinsic p-type semiconductor. Since, the acceptors are formed spontaneously when the Fermi level is high, n-type CZTS is difficult to be realised<sup>155-157</sup>.

As compared to CIGS,  $\text{Cu}_2\text{ZnSnS}_4$  has more potential antisite defects, because the group 13 elements (In and Ga) are replaced by group 12 (Zn) and group 14 (Sn) elements in CZTS. Since the size and valence difference of the Zn and Cu cations are small, the antisite  $\text{Zn}_{\text{Cu}}$  can be easily formed as compared to  $\text{Cu}_{\text{In}}$  and  $\text{Cu}_{\text{Ga}}$  in CIGS<sup>155-157</sup>. Although it is difficult to distinguish between Cu and Zn using standard X-ray diffraction techniques, neutron diffraction has provided direct confirmation of site-disorder in the Cu-Zn sublattice of kesterites<sup>162</sup>. Similarly, other charge-compensated defect complexes, such as  $\text{V}_{\text{Cu}}+\text{Zn}_{\text{Cu}}$ ,  $\text{V}_{\text{Zn}}+\text{Sn}_{\text{Zn}}$ ,  $\text{Cu}_{\text{Sn}}+\text{Sn}_{\text{Cu}}$ , are easy to form, with some experimental signatures of their presence<sup>163,164</sup>. Similar to those in CIGS, charge neutral complexes are expected to passivate deep donor levels and to decrease hole carrier concentrations<sup>155-157</sup>.

CZTS exhibits a structural transition in the Cu/Zn sublattice at a critical temperature around 200 °C<sup>162,165-171</sup>. The transition has been attributed to the disorder of cations, mainly Cu and Zn located at the  $2c$  and  $2d$  Wyckoff positions of the kesterite structure, respectively. DFT calculations predict the antisite defects to be formed in large quantity owing to the low formation energies<sup>155-157</sup>. Monte Carlo simulations showed the disordered cations form a cluster, which leads to a compositional inhomogeneity<sup>172</sup>. Such inhomogeneity results in bandgap fluctuations, which may contribute to the large  $V_{\text{oc}}$  deficit in kesterite solar cells. Scragg *et al*<sup>171</sup> predicted that the disorder introduces spatial bandgap fluctuations in the range of several hundred meV. However, recently, Bourdais *et al*<sup>154</sup> questioned the effect of disorder on the efficiency. They claimed that disorder decreases  $V_{\text{oc}}$

yet increases  $J_{sc}$  so the overall photovoltaic efficiency does not change significantly, as evidenced by samples annealed under a range of conditions.

Photo-generated carrier lifetimes are a major limiting factor of power conversion efficiency in CZTS<sup>173–175</sup> and are shorter than other technologies (see Table 1). One of the primary causes is donor defects trapping minority carriers (electrons). A high concentration of traps result in a reduction in carrier mobility and in turn a reduction in the recombination rate. When donor levels becomes deeper, the captured electrons recombine with holes rather than being slowly released back to the conduction band. During the deep-level recombination process (Box 3), the excess energy is dissipated via multiphonon (heat) emission. Recently, the sulphur vacancy was identified as a possible recombination center in CZTS<sup>176</sup>. However, it is yet unclear which defects act as the main non-radiative recombination centres in CZTS and how they can be removed or suppressed. Again, further theory and experiment are required to shed light on this topic and enhance the performance of kesterite solar cells.

### **Halide perovskites**

Semiconducting metal halides that adopt the perovskite crystal structure have been known since the 1950s<sup>177</sup>, and two decades later the hybrid organic-inorganic halide perovskite  $\text{CH}_3\text{NH}_3\text{PbI}_3$  was reported<sup>178</sup>. The first photovoltaic devices based on  $\text{CH}_3\text{NH}_3\text{PbI}_3$  were in a dye-sensitised solar cell configuration<sup>179</sup>; however, these have since been extended to solid-state mesoporous and thin-film architectures with performance exceeding 22% in small cells<sup>180</sup>. The building blocks of these materials are an anionic framework of corner-sharing lead iodide octahedra ( $\text{PbI}_3^-$ ), with a cation (e.g. caesium, methylammonium or formamidinium) present at the centre of each cuboctahedral cage (see Figure 1g). The upper valence band and lower conduction band are formed by the filled Pb 6s / I 5p and empty Pb 6p orbitals, respectively<sup>181</sup>. The electron and hole effective masses are light ( $m^* < 0.2 m_e$ )<sup>182</sup>. The high-frequency relative dielectric constant of  $\text{CH}_3\text{NH}_3\text{PbI}_3$  is 5, which increases to a static relative dielectric constant of ca. 24, and to a value of ca. 33 when molecular rotations are also included<sup>183</sup>.

$\text{CH}_3\text{NH}_3\text{PbI}_3$  (and related materials) exhibit unusual defect physics. The dominant point defects have been predicted to have shallow levels, which is ideal for photovoltaic applications<sup>184</sup>, and despite being processed at low temperature from solution, carrier mobility and lifetimes are not severely limited by lattice defects. The defect tolerance of the materials has been understood in

terms of the overlap of atomic orbitals and how they form the electronic band edges, in addition to effective dielectric screening<sup>185,186</sup>. In the development of perovskite solar cells, little attention was paid to point defects as high-performance could be achieved using standard processing routes. However, further improvements will require careful control of non-radiative processes that limit  $V_{OC}$  to 0.1–0.2 V below the radiative limit<sup>187</sup>.

Compared to the other systems discussed above, there is limited information available on point defects in halide perovskites. Particular care has to be given to the interpretation of temperature-dependant measurements for these materials as they undergo a number of structural phase transitions and the dielectric permittivity exhibits a strong temperature dependence<sup>183,188</sup>. Concerning defect levels, a thermally stimulated current (TSC) study reported four signals: T1 and T2 were attributed to shallow centres, T3 to a phase transition, and T4 to a trap state at ca. 0.5 eV with a density of  $10^{15} \text{ cm}^{-3}$ <sup>189</sup>. In a recent deep-level transient spectroscopy (DLTS) study of high-performance devices, three peaks were reported: A1 at 0.82 eV, A2 at 0.78 eV and A3 at 0.46 eV below the conduction band<sup>190</sup>. Peaks A1 and A2 were found to have the highest capture cross-section, but were suppressed when the material was processed in an iodine-rich environment. Further caution has to be taken for the interpretation of capacitance features as these materials are mixed-ionic electronic conductors with activation energies for diffusion in an energy range similar to the measured levels,<sup>191</sup> and ion diffusion can also be enhanced upon illumination<sup>192</sup>.

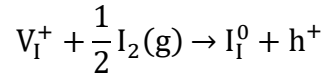
The calculation of accurate defects levels in lead perovskites is problematic as a quantitative description of the electronic structure requires a relativistic description including spin-orbit coupling, which results in a large renormalisation of the bandgap<sup>182,193</sup>. Work by Du highlighted the sensitivity of the predicted defect levels to the choice of electronic structure Hamiltonian<sup>194</sup>. There is agreement that site vacancies involving methylammonium, lead and iodine – predicted to be the dominant point defects<sup>195</sup> – do not result in sub-bandgap levels. Despite the facile ionisation of these donor and acceptor defects, the low carrier concentrations ( $< 10^{15} \text{ cm}^{-3}$ ) that are commonly observed for the lead halide perovskites can be explained by ionic compensation<sup>196</sup>. In the Schottky-limit, the charges of each of the constituent site vacancies cancel:

$$[V_{MA}^-] + [V_{Pb}^{2-}] = 3[V_I^+]$$

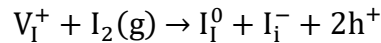
which suppresses the concentrations of free electrons and holes.



The most likely candidate for deep levels is excess iodine in the form of iodine interstitials<sup>197</sup>, which has been shown to be efficient at trapping holes to form H and V centres (driven by I-I bond formation) that have been well established in other metal halide compounds<sup>198,199</sup>. Annealing a perovskite film in excess iodine can fill iodine vacancies resulting in the generation of holes:



or can additionally result in the formation of interstitial defects, for example:



Indeed, treatment using iodine vapour has been found to increase the electrical conductivity and to enhance the hole concentration (the Fermi level can shift more than 100 meV towards the valence band)<sup>200</sup>.

We are far from a clear understanding of defect processes in halide perovskites, in particular relating to the effect of light on defect formation and transport, which are the subject of on-going investigations<sup>201–204</sup>. Beyond processes involving native defects, there has been no clear demonstration of an all-perovskite p-n junction, and currently all high-performance perovskite solar cells employ an intrinsic (low doping level) perovskite layer in p-i-n type configurations. The design and demonstration of effective donor and acceptor dopants would allow for new solar cell architectures and application areas to be realised.

### **Principles for defect control**

Each semiconducting material exhibits a distinct defect and doping selectivity – dictated by the underlying chemical bonding and crystal structure – and much research effort has been invested into understanding the underlying mechanics<sup>186</sup>. In this section, we outline a set of principles concerning defect control in semiconductors for solar cells.

#### *Overcoming doping limits*

In photovoltaic devices, it is necessary to control doping levels and carrier concentrations to fabricate effective semiconductor junctions and tune key material parameters including electrical resistivity, depletion widths, and Fermi level splitting.

Two types of behaviour limit the efficiency of doping: (i) *solubility limits* where the equilibrium concentration of a dopant is too low; and (ii) *charge compensation limits* where the charge of a dopant is cancelled either by a competing configuration (e.g.  $\text{Na}_{\text{Cd}}^-$  vs  $\text{Na}_i^+$  in CdTe) or other native charged point defects in the system (e.g.  $\text{V}_{\text{Cu}}^-$  vs  $\text{In}_{\text{Cu}}^{2+}$  in  $\text{CuInS}_2$ ). Solubility limits can be influenced by the growth conditions (chemical potentials) and even be bypassed by using non-equilibrium synthetic procedures<sup>205</sup>. Charge compensation on other hand is more restrictive: if the formation energy of a compensating defect becomes negative, it will form spontaneously (so-called charge killer defects)<sup>206</sup>. The Fermi level (carrier concentrations) in a semiconductor will be pinned at an energy corresponding to this spontaneous defect formation, and pinning levels have been observed in many compounds<sup>196,207</sup>.

One solution to overcome doping bottlenecks of semiconductors is by tuning the processing conditions. For a binary material, AB, formed of a cation  $\text{A}^+$  and anion  $\text{B}^-$ , n-type (electron) doping will require the suppression of  $\text{V}_{\text{A}}^-$  defects and therefore cation-rich growth conditions. Conversely, p-type (hole) doping will require the suppression of  $\text{V}_{\text{B}}^+$  defects and therefore anion-rich growth conditions<sup>208,209</sup>. In the context of halide perovskites, p-type doping could be achieved by replacing some lattice  $\text{Pb}^{2+}$  by  $\text{Ag}^+$  forming  $\text{Ag}_{\text{Pb}}^-$ ; however, it would be necessary to prevent the formation of compensating iodine vacancies. While a condition of hole compensation is desired, i.e.  $[\text{Ag}_{\text{Pb}}^-] = [\text{h}^+]$ , spontaneous iodine loss is likely to result in a condition of  $[\text{Ag}_{\text{Pb}}^-] = [\text{V}_{\text{I}}^+]$ , which negates the effect of acceptor doping. One solution is to simultaneously introduce a dopant while controlling the iodine chemical potential, e.g. processing the acceptor-doped material in an I-rich atmosphere. In this way, it may be possible to develop robust p-type and n-type halide perovskites.

A second solution is to choose an alternative host compound with a more favourable electronic structure. It has been observed that p-type doping is favoured in materials with “high” valence bands close to the vacuum level, and n-type doping is favoured in materials with “low” conduction bands<sup>210</sup>. This behaviour can be understood simply from a low ionisation potential (energy associated with electron removal) facilitating hole formation, and a high electron affinity (energy associated with electron addition) stabilising excess electrons<sup>211</sup>. The band energies of a semiconductor can be controlled either with chemistry (compositional engineering) or structure (crystal engineering). For example, a valence band more amenable to p-type doping can be

achieved by incorporating ions with low-binding energy valence orbitals such as Cu(I) 3d<sup>10</sup>, Ag(I) 4d<sup>10</sup>, Sn 5s<sup>2</sup> and Pb 6s<sup>2</sup>, whereas it has been shown the valence band of TiO<sub>2</sub> can be modified by several eV simply by changing the polymorph (e.g. from rutile to anatase or brookite)<sup>212</sup>.

### *Enhancing carrier lifetime*

The lifetime of charge carriers in solar cells can be as essential as the doping efficiency. The development of Si technology has shown the importance of intrinsic defects and dopants,<sup>16</sup> unintentional extrinsic impurities,<sup>28</sup> and defects formed under operating conditions<sup>52,59</sup> in achieving high light-to-electricity conversion efficiency.

Carrier lifetime is reduced by trapping in deep defect centres and ultimately through recombination between electrons and holes. Solar cells usually operate in a low carrier density regime ( $n < 10^{17}$  cm<sup>-3</sup>) where monomolecular recombination dominates; therefore, careful control of the concentration of deep level defects is essential (see Box 3). The physical process of non-radiative defect-assisted recombination is complex and couples the electronic and vibrational states of a material, so there are few established guidelines. In Si, chemical passivation is used to remove dangling bonds, whereas in CIGS, defect-defect interactions forming charge-neutral clusters serve to remove deep electron and hole traps. Recently, there has been significant progress in the first-principles description of the capture cross-section and recombination rates for point defects in semiconductors<sup>176,213,214</sup>, which may enable the development of new structure-property maps and design procedures and principles in the near future.

Practically, photo-generated carrier lifetime is enhanced not only by the removal of the defects and impurities, but also through changes in the device architecture. Several approaches have been pioneered in Si-technologies such as spatial modulation of the Fermi level with back-surface fields<sup>215</sup> and heavily-doped regions near the electrical contacts<sup>14</sup>. The former is to reduce the density of recombination sites and the latter is to reduce the spatial overlap between the defects and charge carriers.

Other solar cell technologies share the same fundamental working principles as Si, and thus these concepts can be adapted to enhance performance. For instance, the concept of the spatial separation of charge carriers and recombination sites has been realized in CIGS<sup>216</sup> using a gradient in the In:Ga composition ratio, which raises the conduction band of the absorber material near the contacts and reduces interface recombination rates. More recently, the company First Solar

developed bandgap graded CdTe solar cells<sup>217</sup> using a Cd(Se,Te) absorber layer. This approach could be adapted for CZTS, e.g. through the use of (Ag,Cu), (Zn,Cd) or (S,Se) chemical gradients. Halide perovskites and newly emerging systems such as SnS, CuSbS<sub>3</sub>, and FeS<sub>2</sub> may so benefit from these advances to overcome their high-recombination rates and low cell voltages. For example, SnS has a bandgap of 1.1 eV which makes it comparable to Si, yet the champion solar cell efficiency is below 5% and the  $V_{oc}$  is only 0.4 V.<sup>218</sup> The minority carrier lifetime of SnS has been recently improved from < 1 ns to > 3 ns by avoiding low concentrations of avoiding extrinsic impurities,<sup>219</sup> which has not solved the problem but illustrates the importance of defect engineering.

## Outlook

In the search for new photovoltaic materials, the magnitude of the bandgap and visible-range absorption spectrum are useful selection metrics<sup>220–222</sup>. We argue that consideration of point defect processes is just as essential. While a material may absorb sunlight, the presence of detrimental defects can severely hinder its ability to generate and transport photo-generated charge carriers. There is an abundance of materials with bandgaps in the visible range (1 – 3 eV), which make them attractive from consideration of the theoretical Shockley-Queisser limit, but very few classes of semiconductors have resulted in photovoltaic efficiencies above 10%. This is due both to the inability to control the equilibrium concentrations of electrons and holes (limits to doping) and the presence of efficient non-radiative pathways often involving sub-bandgap electronic states introduced by intrinsic defects and extrinsic impurities (low carrier lifetimes).

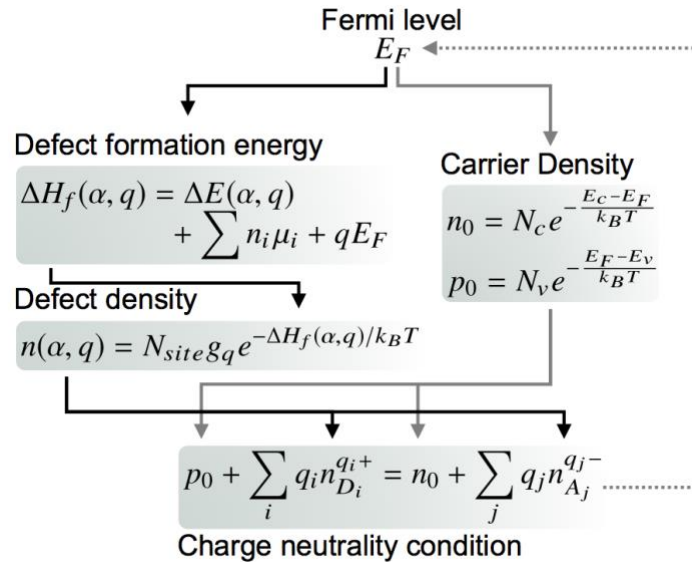
The defect physics and chemistry of novel materials should be carefully assessed to screen and predict plausible high-efficiency photovoltaic materials. Indeed, defect tolerance has been proposed as a guiding principle for discovering new compounds<sup>185,223–226</sup>. However, the wide range of defect levels and processes found in current technologies (Table 2) show that they are not naturally defect tolerant, but rather processing routes and chemical treatments have been carefully developed over time to minimize the effects of the most detrimental species. We recognize that point defects are much harder to screen, measure and predict compared to bandgaps; however, we suggest that close collaboration between theoretical and experimental investigators, and between academic and industrial researchers, is required to develop more realistic and robust design procedures for next-generation solar energy solutions.

## **Acknowledgements**

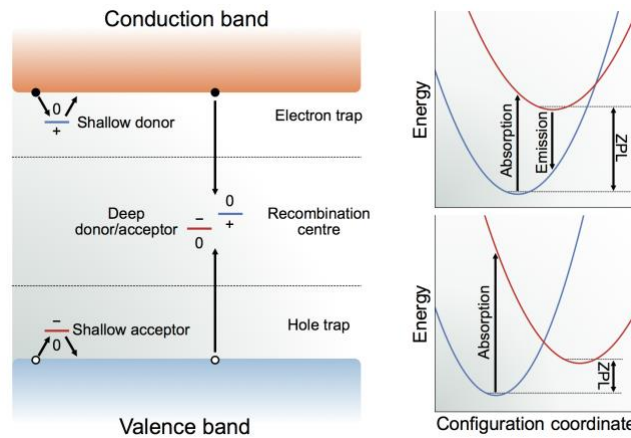
The authors thank Su-Huai Wei, Kee Joo Chang, Alex Zunger, Alexey Sokol, and Chris van de Walle for illuminating discussions regarding defects in semiconductors. This project has received funding from the European H2020 Framework Programme for research, technological development and demonstration under grant agreement no. 720907. See <http://www.starcell.eu>. AW is supported by a Royal Society University Research Fellowship and the Leverhulme Trust, while JP is supported by a Royal Society Shooter Fellowship.

Box 1 | **Equilibrium thermodynamics of point defect formation.** The thermodynamic driving force for the formation of point defects in crystalline materials is configurational entropy. While perturbing the order of a crystal requires enthalpy (H), the overall free energy of a crystal (G) is lowered by the gain in entropy (S):  $G = H - TS$ . Minimising the free energy of a crystal with respect to the concentration of a defect ( $n_d$ ) yields a simple expression:  $n_d = N_{site} g_q e^{(-\frac{\Delta H_f}{k_B T})}$ , where  $N$  are the number of lattice sites,  $g$  represents a degeneracy factor (e.g. spin states), and  $\Delta H_f$  represents the formation enthalpy of the point defect.

The reality of imperfect semiconductors is more complex for a system with a range of defects in a variety of charge states ( $q$ ). The concentrations of electrons [ $n$ ] and holes [ $p$ ] must balance the concentration of charged donors ( $D$ ) and acceptors ( $A$ ):  $[p^+] + [D^+] = [n^-] + [A^-]$ . In modern defect theory, the equilibrium concentrations of defects can be calculated self-consistently by determining the Fermi level ( $E_F$ ) of the system under the constraint of overall charge neutrality. It has become commonplace to calculate such quantities using first-principles techniques; however, further advances are needed to incorporate finite-temperature effects (e.g. vibrational entropy and thermal expansion) and to more realistically simulate experimental growth conditions (e.g. thermodynamic activity of gases and solvents).



Box 2 | **Classification of defect levels in semiconductors.** When a crystal of Si is doped with P, the system gains an excess electron owing to the higher atomic number of the impurity atom. This excess electron could remain trapped at the substitutional defect site (neutral state of the defect) or could be donated to the conduction band of the host material (charged state of the defect) and become a free charge carrier. The energy difference between the charged and neutral states of the defect correspond to the ionisation level with respect to the conduction band, i.e.  $P_{Si}^0 \rightarrow P_{Si}^+ + e^-$ . For B, which contains one electron less than Si, an equivalent acceptor level can be defined with respect to the valence band of the host material ( $B_{Si}^0 \rightarrow B_{Si}^- + h^+$ ).



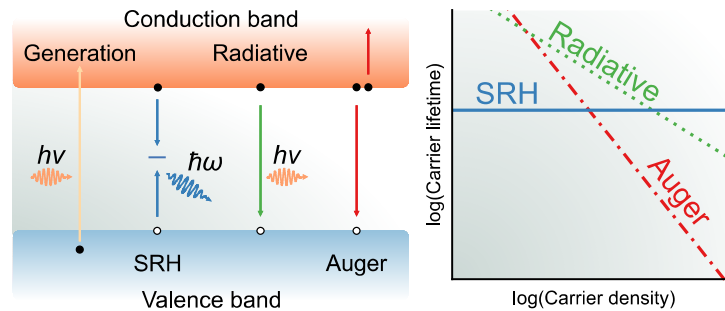
Defects that introduce levels close ( $E < k_B T \sim 25 \text{ meV}$  at  $T = 300 \text{ K}$ ) to the valence or conduction bands are termed *shallow* and are effective at generating free charge carriers. The label of a defect as shallow can also imply that the associated electronic wavefunction is delocalised and hydrogenic. Defects that introduce levels *deep* in the bandgap ( $E > k_B T$ ) can still be activated optically, and can also act as effective intermediate states for electron-hole generation or recombination. Deep levels are often associated with a large lattice distortion and an electronic wavefunction that is localised on a single atom or a small group of atoms. If the defect wavefunction overlaps with the continuum of valence or conduction bands it is termed a *resonant* state, which may still be optically active.

It is important to make a distinction between two types of defect level: *optical* levels correspond to fast (vertical Franck–Condon processes with no response in the local atomic structure) with the absorption or emission of a photon; and *thermal* levels that correspond to the transition between two energy minima on a potential energy surface (including the effects of structural relaxation). The energy surfaces of a defect are often shown in the form of configuration coordinate diagrams,

which contain information on both optical absorption and emission processes, as well as the thermal transition in the form of the zero-phonon line (ZPL). The configuration coordinate (y axis) refers to a combination of lattice vibrations (phonons) involved in the local relaxation of the defect centre. Defects with weak coupling to the lattice show a small shift in the ground and excited state potential energy surfaces and can be expected to be active for luminescence. Strong coupling to lattice distortions result in a large shift in configuration coordinate, suppressing luminescence and promoting non-radiative transitions accompanied by multiphonon (heat) emission to the lattice.



Box 3 | **Electron-hole recombination in solar cells.** When a semiconductor interacts with light, photons with energy higher than the bandgap can excite an electron from the valence band into the conduction band, thereby generating an exciton that dissociates into a free electron and hole pair. The photogenerated electron and hole carriers collected at the p-n junction produce the current in a photovoltaic device. Therefore, carrier lifetime is one of the most important parameters that determines the performances of solar cells. Carrier lifetime is limited by the rate of electron-hole recombination, which can be radiative (with light emission) or non-radiative (with only phonon emission). The kinetics of the decay in the concentration ( $n$ ) of photogenerated charge carriers is often modelled using a third-order rate equation of the form  $\frac{dn}{dt} = G - k_1n - k_2n^2 - k_3n^3$ , where charge-carrier generation ( $G$ ) is offset by one-particle ( $k_1$ ), two-particle ( $k_2$ ) and three-particle ( $k_3$ ) recombination processes. The contribution from each process to the total recombination is sensitive to the carrier density (illumination intensity).



In a low carrier density regime ( $n < 10^{15} \text{ cm}^{-3}$ ), deep-level non-radiative recombination is often the dominant recombination mechanism. A deep level in the bandgap of a semiconductor provides an intermediate state that facilitates the sequential capture of minority and majority carriers, which can be described by Shockley-Read-Hall (SRH) statistics. The recombination becomes an effectively first-order process ( $k_1$ ) as the kinetics are usually limited by the capture of the minority carrier. During the recombination process – which may occur in the bulk material, as well as at surfaces or interfaces – the energy is dissipated via emitting heat in the form of phonons (lattice vibrations).

At the intermediate carrier densities, two-particle band-to-band recombination ( $k_2$ ) processes becomes important, where photogenerated electron and holes recombine directly by emitting photons. This is an unavoidable thermodynamic loss required by the symmetry of light absorption and emission processes (detailed balance). For valence-to-conduction band recombination, the

emitted photons can be reabsorbed by the material, which is termed photon recycling. For indirect bandgap semiconductors values of  $k_2$  are smaller than for direct bandgap materials, which places increased weight on  $k_1$  and  $k_3$  processes.

In Auger recombination, a carrier collides with a second carrier of the same type. Following the collision, one carrier gains kinetic energy, being excited to a higher energy state, while the other carrier recombines with a third carrier of opposite type. Since three particles are involved, Auger recombination ( $k_3$ ) generally limits the carrier lifetime significantly only in very high carrier density regime ( $n > 10^{17} \text{ cm}^{-3}$ ), but in the case of high-quality (low defect density) Si it is a limiting process under solar illumination.

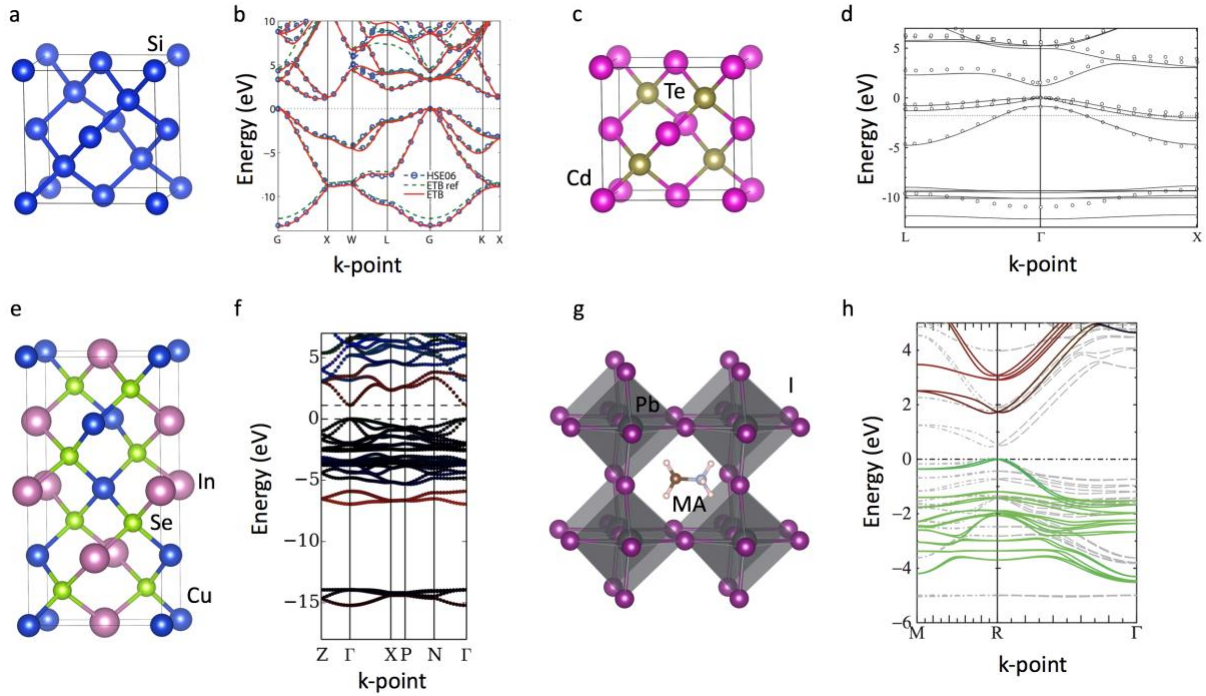


Figure 1 | **Crystal structure and electronic band structure of Si, CdTe, CuInSe<sub>2</sub> and CH<sub>3</sub>NH<sub>3</sub>PbI<sub>3</sub>.** a) Si in the diamond structure. b) Electronic band structure of bulk Si calculated using DFT with the HSE06 functional (open circle), and that obtained by empirical tight-binding (ETB) models. c) CdTe in the zinc-blende structure. d) Band structure of CdTe calculated using DFT/HSE06 (solid line) and empirical nonlocal scheme (open circle). e) Conventional unit cell for the chalcopyrite CuInSe<sub>2</sub>. f) Band structure of CuInSe<sub>2</sub> in the body-centred tetragonal primitive cell from DFT/HSE06. Red, blue, and green colours represent the percentage of s, p, and d orbitals of In. g) Atomic structure of cubic CH<sub>3</sub>NH<sub>3</sub>PbI<sub>3</sub>. h) Quasiparticle self-consistent *GW* band structure (solid line) of the lead halide perovskite. Green, red, and blue depict I 5p, Pb 6p, Pb 6s, respectively. DFT/LDA band structure (dashed line) is shown for comparison. The valence band maximum is set to 0 eV in panel b, d, f and h. Panel b is adapted with permission from Ref. <sup>227</sup>, APS. Panel d is adapted with permission from Ref. <sup>228</sup>, Elsevier. Panel f is adapted with permission from Ref. <sup>229</sup>, AIP. Panel h is adapted with permission from Ref. <sup>230</sup>, APS.

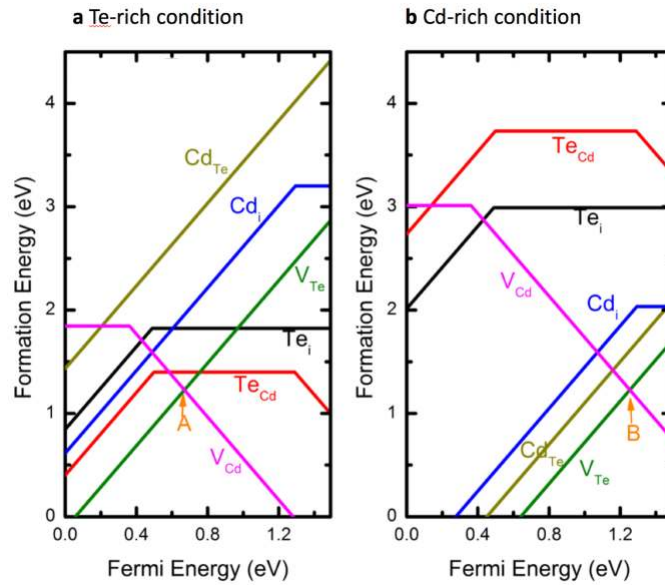


Figure 2 | **Formation energy of intrinsic point defects in CdTe under (a) Te-rich and (b) Cd-rich conditions.** Only the most stable charge states of each defect are shown for clarity. The levels **A** and **B** denote the predicted Fermi level pinning energy under equilibrium growth conditions. The deep acceptor level of Cd vacancy ( $\text{V}_{\text{Cd}}$ ) and the low formation energy of Te vacancy ( $\text{V}_{\text{Te}}$ ) make it difficult to achieve p-type CdTe with a high hole concentration. The image is adapted with permission from Ref. <sup>71</sup>, APS.

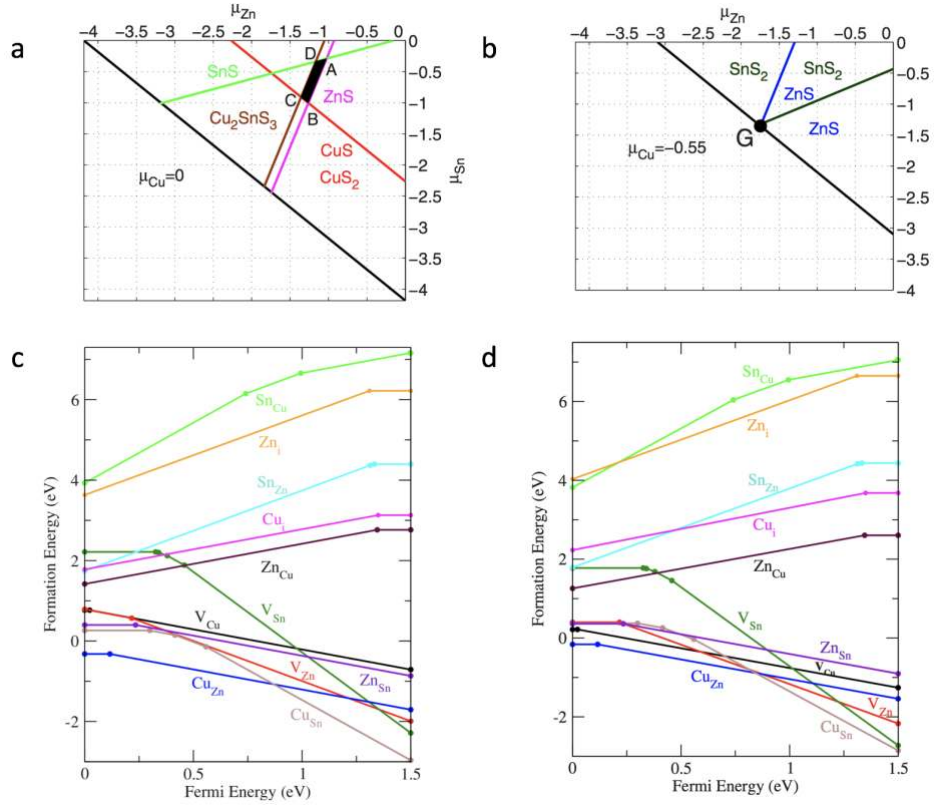


Figure 3 | **Atomic chemical potentials that stabilise the formation of quaternary kesterite  $\text{Cu}_2\text{ZnSnS}_4$  (CZTS) and formation energy of point defects under two growth conditions.** The stability condition of the material with respect to its elements ( $2\mu_{\text{Cu}} + \mu_{\text{Zn}} + \mu_{\text{Sn}} + \mu_{\text{S}} < \Delta H_f$ ) is further constrained by the formation of secondary phases. In panel a, CZTS becomes stable than its secondary phases in the blackened area, which is surrounded by several lines in which both CZTS and a secondary phase can be formed. The intersection points of the lines are denoted A–D. In panel b, CZTS can be only formed at condition G because of low chemical potential of Cu. Panel c and d show the formation energy of native defects in CZTS under conditions C (Cu-rich) and G (Cu-poor). The panels are adapted with permission from Ref. <sup>156</sup>, APS.

**Table 1. Comparison of Si and thin-film photovoltaic technologies.** Efficiency relates to the record light-to-electricity conversion achieved in a photovoltaic device of at least 1 cm<sup>2</sup> from Ref. <sup>51</sup>. CIGS relates to Cu(In,Ga)(S,Se)<sub>2</sub>, CZTS relates to Cu<sub>2</sub>ZnSn(S,Se)<sub>4</sub>, while halide perovskite relates to CH<sub>3</sub>NH<sub>3</sub>PbI<sub>3</sub>.

| <b>Technology</b> | <b>Efficiency (%)</b> | <b>Doping type</b> | <b>Extrinsic dopants</b> | <b>Common point defects</b>   | <b>Minority carrier lifetime</b> |
|-------------------|-----------------------|--------------------|--------------------------|---|----------------------------------|
| Si                | 26.7                  | p or n             | B, P, Al <sup>14</sup>   | Si dangling bonds, transition metals, B-O complexes                 | 8.8 ms <sup>57</sup>             |
| CdTe              | 21.0                  | p or n             | Cu, Cl, P                | V <sub>Cd</sub> , V <sub>Te</sub> , Te <sub>Cd</sub> , Te-Te        | 1 ns – 30 ns <sup>102</sup>      |
| CIGS              | 21.7                  | p                  | -                        | V <sub>Cu</sub> , (In,Ga) <sub>Cu</sub>                             | 10 – 100 ns <sup>231</sup>       |
| CZTS              | 10.0                  | p                  | -                        | V <sub>Cu</sub> , Zn <sub>Cu</sub> , Cu <sub>Zn</sub>               | < 1 ns <sup>175</sup>            |
| Halide perovskite | 20.9                  | p or n             | -                        | V <sub>Pb</sub> , V <sub>I</sub> , V <sub>MA</sub> , I <sub>i</sub> | 100 – 1000 ns <sup>232–235</sup> |

**Table 2. Sub-bandgap defect levels reported in Si, CdTe, CIGS, and halide perovskite.** Positive and negative values of transition levels denote the transition level with respect to the valence band maximum and the conduction band minimum of the pristine host material, respectively.

| <b>Technology</b>    | <b>Defect</b>                    | <b>Transition level</b>  | <b>Reference</b>    |
|----------------------|----------------------------------|--|---------------------|
| Si                   | Si dangling bond                 | 0.31 (1+/0), 0.80 (0/1-)   | expt <sup>236</sup> |
|                      | V <sub>Si</sub>                  | 0.08 (2+/0), 0.91 (0/2-)   | calc <sup>50</sup>  |
|                      | B-O complex                      | 0.34, 0.38, 0.41 (donor)<br>0.26, 0.28, 0.31 (acceptor)                      | expt <sup>54</sup>  |
|                      | Cu <sub>Si</sub>                 | 0.20 (1+/0), 0.54 (0/1-), 0.97 (1-/2-)                                       | calc <sup>44</sup>  |
| CdTe                 | V <sub>Cd</sub>                  | 0.36 (0/2-)  | calc <sup>67</sup>  |
|                      | Te <sub>Cd</sub>                 | 0.50 (2+/0), 1.29 (0/2-)   | calc <sup>67</sup>  |
|                      | Cl <sub>Te</sub>                 | 1.3 (1+/0)   | calc <sup>67</sup>  |
|                      | unclassified                     | 0.12, 0.14, 0.15, 0.20, 0.25, 0.32, 0.43,<br>0.57, -0.64, 0.76, -0.79, -1.10 | expt <sup>87</sup>  |
| CIGS                 | V <sub>Cu</sub>                  | 0.08 (0/1-)  | calc <sup>237</sup> |
|                      | In <sub>Cu</sub>                 | 0.86 (2+/0)  | calc <sup>237</sup> |
|                      | V <sub>Se</sub>                  | 0.52 (2+/0)  | calc <sup>237</sup> |
|                      |                                  | 0.08 (2+/0), 0.98 (0/1-)   | calc <sup>117</sup> |
|                      | V <sub>Se</sub> -V <sub>Cu</sub> | 0.29 (1+/1-) 0.86 (1-/2-)  | calc <sup>117</sup> |
|                      | unclassified                     | 0.6, 0.81, 0.1-0.4, 0.45-0.58, 0.33,<br>0.3, 0.07                            | expt <sup>238</sup> |
| Halide<br>perovskite | I <sub>i</sub>                   | 0.15 (0/1-), 0.58 (1+/1-), 1.01 (1+/0)                                       | calc <sup>194</sup> |
|                      | I <sub>MA</sub>                  | 0.17 (1-/2-), 0.54 (0/2-), 0.91 (0/1-)                                       | calc <sup>194</sup> |
|                      | unclassified                     | -0.46, -0.78, -0.82  | expt <sup>190</sup> |

## References

1. Pantelides, S. T. The electronic structure of impurities and other point defects in semiconductors. *Rev. Mod. Phys.* **50**, 797 (1978).
2. Stoneham, A. M. *Theory of Defects in Solids*. (OUP Oxford, 1975).
3. Frenkel, J. Über die Wärmebewegung in festen und flüssigen Körpern. *Zeitschrift für Phys.* **35**, 652 (1926).
4. Kroger, F. A. & Vink, H. J. Relations between the concentrations of imperfections in solids. *J. Phys. Chem. Solids* **5**, 208–223 (1958).
5. Mott, N. F. & Littleton, M. J. Conduction in polar crystals. I. Electrolytic conduction in solid salts. *Trans. Faraday Soc.* **34**, 485 (1938).
6. Freysoldt, C. *et al.* First-principles calculations for point defects in solids. *Rev. Mod. Phys.* **86**, 253 (2014).
7. Bracht, H., Haller, E. E. & Clark-Phelps, R. Silicon Self-Diffusion in Isotope Heterostructures. *Phys. Rev. Lett.* **81**, 393–396 (1998).
8. Gartsman, K. *et al.* Direct evidence for diffusion and electromigration of Cu in CuInSe<sub>2</sub>. *J. Appl. Phys.* **82**, 4282–4285 (1997).
9. Istratov, A. A., Flink, C., Hieslmair, H., Weber, E. R. & Heiser, T. Intrinsic Diffusion Coefficient of Interstitial Copper in Silicon. *Phys. Rev. Lett.* **81**, 1243–1246 (1998).
10. Eames, C. *et al.* Ionic transport in hybrid lead iodide perovskite solar cells. *Nat. Commun.* **6**, 7497 (2015).
11. Buckeridge, J. *et al.* Determination of the nitrogen vacancy as a shallow compensating center in GaN doped with divalent metals. *Phys. Rev. Lett.* **114**, 16405 (2015).
12. Madelung, O. M. *Semiconductors: Data Handbook*. (Springer, 2003).
13. De Wolf, S., Descoedres, A., Holman, Z. C. & Ballif, C. High-efficiency Silicon Heterojunction Solar Cells: A Review. *Green* **2**, (2012).
14. Battaglia, C., Cuevas, A. & De Wolf, S. High-efficiency crystalline silicon solar cells: status and perspectives. *Energy Environ. Sci.* **9**, 1552–1576 (2016).
15. Newman, R. C. Defects in silicon. *Reports Prog. Phys.* **45**, 1163–1210 (1982).
16. Fahey, P. M., Griffin, P. B. & Plummer, J. D. Point defects and dopant diffusion in silicon. *Rev. Mod. Phys.* **61**, 289–384 (1989).
17. Adachi, D., Hernández, J. L. & Yamamoto, K. Impact of carrier recombination on fill factor for large area heterojunction crystalline silicon solar cell with 25.1% efficiency. *Appl. Phys. Lett.* **107**, 233506 (2015).
18. Pankove, J. I. & Tarnag, M. L. Amorphous silicon as a passivant for crystalline silicon. *Appl. Phys. Lett.* **34**, 156–157 (1979).
19. Aberle, A. G. Surface passivation of crystalline silicon solar cells: a review. *Prog. Photovoltaics Res. Appl.* **8**, 473–487 (2000).
20. Richter, A., Hermle, M. & Glunz, S. W. Crystalline Silicon Solar Cells Reassessment of the Limiting Efficiency for Crystalline Silicon Solar Cells. *IEEE J. Photovoltaics* **3**, 1184–1191 (2013).
21. Broqvist, P., Alkauskas, A. & Pasquarello, A. Defect levels of dangling bonds in silicon and germanium through hybrid functionals. *Phys. Rev. B* **78**, 75203 (2008).
22. George, B. M. *et al.* Atomic structure of interface states in silicon heterojunction solar cells. *Phys. Rev. Lett.* **110**, 1–5 (2013).
23. Higashi, G. S., Chabal, Y. J., Trucks, G. W. & Raghavachari, K. Ideal hydrogen termination of the Si (111) surface. *Appl. Phys. Lett.* **56**, 656–658 (1990).
24. Chang, K. J. & Chadi, D. J. Hydrogen bonding and diffusion in crystalline silicon. *Phys. Rev. B* **40**, 11644 (1989).



25. Hoex, B., Gielis, J. J. H., Van De Sanden, M. C. M. & Kessels, W. M. M. On the c-Si surface passivation mechanism by the negative-charge-dielectric Al<sub>2</sub>O<sub>3</sub>. *J. Appl. Phys.* **104**, 113703 (2008).
26. Davis, J. R. *et al.* Impurities in silicon solar cells. *IEEE Trans. Electron Devices* **27**, 677–687 (1980).
27. Coletti, G. *et al.* Impact of Metal Contamination in Silicon Solar Cells. *Adv. Funct. Mater.* **21**, 879–890 (2011).
28. Peaker, A. R. *et al.* Recombination via point defects and their complexes in solar silicon. *Phys. Status Solidi Appl. Mater. Sci.* **209**, 1884–1893 (2012).
29. Gilles, D., Schröter, W. & Bergholz, W. Impact of the electronic structure on the solubility and diffusion of 3d transition elements in silicon. *Phys. Rev. B* **41**, 5770 (1990).
30. Zimmermann, H. & Ryssel, H. Gold and Platinum Diffusion - the Key To the Understanding of Intrinsic Point-Defect Behavior in Silicon. *Appl. Phys. a-Materials Sci. Process.* **55**, 121–134 (1992).
31. Lemke, H. Properties of Silicon Crystals Doped with Zirconium or Hafnium. *Phys. Status Solidi* **122**, 617–630 (1990).
32. Istratov, A. A., Buonassisi, T., Pickett, M. D., Heuer, M. & Weber, E. R. Control of metal impurities in ‘dirty’ multicrystalline silicon for solar cells. *Mater. Sci. Eng. B* **134**, 282–286 (2006).
33. Hofstetter, J., Lelièvre, J. F., del Cañizo, C. & Luque, A. Acceptable contamination levels in solar grade silicon: From feedstock to solar cell. *Mater. Sci. Eng. B Solid-State Mater. Adv. Technol.* **159–160**, 299–304 (2009).
34. Pizzini, S. Towards solar grade silicon: Challenges and benefits for low cost photovoltaics. *Sol. Energy Mater. Sol. Cells* **94**, 1528–1533 (2010).
35. Angèle Reinders, Pierre Verlinden, Wilfried van Sark, A. F. *Photovoltaic Solar Energy: From Fundamentals to Applications*. (John Wiley & Sons, 2017).
36. Weber, E. R. Transition metals in silicon. *Appl. Phys. A Solids Surfaces* **30**, 1–22 (1983).
37. Myers, S. M., Seibt, M. & Schröter, W. Mechanisms of transition-metal gettering in silicon. *J. Appl. Phys.* **88**, 3795 (2000).
38. Rein, S. & Glunz, S. W. Electronic properties of interstitial iron and iron-boron pairs determined by means of advanced lifetime spectroscopy. *J. Appl. Phys.* **98**, (2005).
39. Istratov, A. A. *et al.* Nickel solubility in intrinsic and doped silicon. *J. Appl. Phys.* **97**, 23505 (2005).
40. Diez, S., Rein, S., Roth, T. & Glunz, S. W. Cobalt related defect levels in silicon analyzed by temperature- and injection-dependent lifetime spectroscopy. *J. Appl. Phys.* **101**, 33710 (2007).
41. Steger, M. *et al.* Photoluminescence of deep defects involving transition metals in Si: New insights from highly enriched <sup>28</sup>Si. *Journal of Applied Physics* **110**, 81301 (2011).
42. Markevich, V. P. *et al.* Titanium in silicon: Lattice positions and electronic properties. *Appl. Phys. Lett.* **104**, 152105 (2014).
43. Marinopoulos, A. G., Santos, P. & Coutinho, J. DFT+ U study of electrical levels and migration barriers of early 3d and 4d transition metals in silicon. *Phys. Rev. B* **92**, 75124 (2015).
44. Sharan, A., Gui, Z. & Janotti, A. Hybrid-Functional Calculations of the Copper Impurity in Silicon. *Phys. Rev. Appl.* **8**, 24023 (2017).
45. Buonassisi, T. *et al.* Engineering metal-impurity nanodefects for low-cost solar cells. *Nat. Mater.* **4**, 676–679 (2005).
46. Pickett, M. D. & Buonassisi, T. Iron point defect reduction in multicrystalline silicon solar cells. *Appl. Phys. Lett.* **92**, 2006–2009 (2008).
47. Lindroos, J. *et al.* Nickel: A very fast diffuser in silicon. *J. Appl. Phys.* **113**, 204906 (2013).
48. Rinke, P., Janotti, A., Scheffler, M. & Van de Walle, C. Defect Formation Energies without the Band-Gap Problem: Combining Density-Functional Theory and the GW Approach for the Silicon Self-Interstitial. *Phys.*

- Rev. Lett.* **102**, 26402 (2009).
49. Estreicher, S. K., Backlund, D. J., Carbogno, C. & Scheffler, M. Activation energies for diffusion of defects in silicon: The role of the exchange-correlation functional. *Angew. Chemie - Int. Ed.* **50**, 10221–10225 (2011).
  50. Śpiewak, P. & Kurzydłowski, K. J. Formation and migration energies of the vacancy in Si calculated using the HSE06 range-separated hybrid functional. *Phys. Rev. B* **88**, 195204 (2013).
  51. Green, M. A. *et al.* Solar cell efficiency tables (version 51). *Prog. Photovoltaics Res. Appl.* **26**, 2–12 (2018).
  52. Lindroos, J. & Savin, H. Review of light-induced degradation in crystalline silicon solar cells. *Sol. Energy Mater. Sol. Cells* **147**, 115–126 (2016).
  53. Niewelt, T., Schon, J., Warta, W., Glunz, S. W. & Schubert, M. C. Degradation of Crystalline Silicon Due to Boron–Oxygen Defects. *IEEE J. Photovoltaics* **7**, 383–398 (2017).
  54. Hallam, B. *et al.* Recent insights into boron-oxygen related degradation: Evidence of a single defect. *Sol. Energy Mater. Sol. Cells* **173**, 25–32 (2017).
  55. Taguchi, M. *et al.* 24.7% Record efficiency HIT solar cell on thin silicon wafer. *IEEE J. Photovoltaics* **4**, 96–99 (2014).
  56. Masuko, K. *et al.* Achievement of More Than 25% Conversion Efficiency With Crystalline Silicon Heterojunction Solar Cell. *IEEE J. Photovoltaics* **4**, 1433–1435 (2014).
  57. Yoshikawa, K. *et al.* Silicon heterojunction solar cell with interdigitated back contacts for a photoconversion efficiency over 26%. *Nat. Energy* **2**, 17032 (2017).
  58. Boulfrad, Y. *et al.* Experimental evidence on removing copper and light-induced degradation from silicon by negative charge. *Appl. Phys. Lett.* **105**, 182108 (2014).
  59. Luo, W. *et al.* Potential-induced degradation in photovoltaic modules: a critical review. *Energy Environ. Sci.* **10**, 43–68 (2017).
  60. Wei, S.-H., Zhang, S. B. & Zunger, A. First-principles calculation of band offsets, optical bowings, and defects in CdS, CdSe, CdTe, and their alloys. *J. Appl. Phys.* **87**, 1304–1311 (2000).
  61. Ma, J. *et al.* Dependence of the Minority-Carrier Lifetime on the Stoichiometry of CdTe Using Time-Resolved Photoluminescence and First-Principles Calculations. *Phys. Rev. Lett.* **111**, 67402 (2013).
  62. Kranz, L. *et al.* Doping of polycrystalline CdTe for high-efficiency solar cells on flexible metal foil. *Nat. Commun.* **4**, (2013).
  63. Gessert, T. A. *et al.* Research strategies toward improving thin-film CdTe photovoltaic devices beyond 20% conversion efficiency. *Sol. Energy Mater. Sol. Cells* **119**, 149–155 (2013).
  64. Reese, M. O. *et al.* Intrinsic surface passivation of CdTe. *J. Appl. Phys.* **118**, (2015).
  65. Burst, J. M. *et al.* CdTe solar cells with open-circuit voltage breaking the 1 V barrier. *Nat. Energy* **1**, 16015 (2016).
  66. Kanevce, A., Reese, M. O., Barnes, T. M., Jensen, S. A. & Metzger, W. K. The roles of carrier concentration and interface, bulk, and grain-boundary recombination for 25% efficient CdTe solar cells. *J. Appl. Phys.* **121**, (2017).
  67. Yang, J.-H., Yin, W.-J., Park, J.-S., Ma, J. & Wei, S.-H. Review on first-principles study of defect properties of CdTe as a solar cell absorber. *Semicond. Sci. Technol.* **31**, 83002 (2016).
  68. Shepidchenko, A., Sanyal, B., Klintonberg, M. & Mirbt, S. Small hole polaron in CdTe: Cd-vacancy revisited. *Sci. Rep.* **5**, 14509 (2015).
  69. Lindström, A., Mirbt, S., Sanyal, B. & Klintonberg, M. High resistivity in undoped CdTe: carrier compensation of Te antisites and Cd vacancies. *J. Phys. D. Appl. Phys.* **49**, 35101 (2016).
  70. Yang, J. H., Yin, W. J., Park, J. S., Metzger, W. & Wei, S. H. First-principles study of roles of Cu and Cl in polycrystalline CdTe. *J. Appl. Phys.* **119**, (2016).

71. Yang, J. H. *et al.* Tuning the Fermi level beyond the equilibrium doping limit through quenching: The case of CdTe. *Phys. Rev. B* **90**, 245202 (2014).
72. Pautrat, J. L., Francou, J. M., Magnea, N., Molva, E. & Saminadayar, K. Donors and acceptors in tellurium compounds; The problem of doping and self-compensation. *J. Cryst. Growth* **72**, 194–204 (1985).
73. Said, M. & Kanehisa, M. A. Excited states of acceptors in CdTe and ZnTe. *J. Cryst. Growth* **101**, 488–492 (1990).
74. Poplawsky, J. D. *et al.* Direct Imaging of Cl- and Cu-Induced Short-Circuit Efficiency Changes in CdTe Solar Cells. *Adv. Energy Mater.* **4**, 1400454 (2014).
75. Kuciauskas, D. *et al.* The impact of Cu on recombination in high voltage CdTe solar cells. *Appl. Phys. Lett.* **107**, 243906 (2015).
76. Kuciauskas, D. *et al.* Recombination analysis in cadmium telluride photovoltaic solar cells with photoluminescence spectroscopy. *IEEE J. Photovoltaics* **6**, 313–318 (2016).
77. Yang, J. H., Metzger, W. K. & Wei, S. H. Carrier providers or killers: The case of Cu defects in CdTe. *Appl. Phys. Lett.* **111**, 42106 (2017).
78. Yang, J.-H., Park, J.-S., Kang, J. & Wei, S.-H. First-principles multiple-barrier diffusion theory: The case study of interstitial diffusion in CdTe. *Phys. Rev. B* **91**, 75202 (2015).
79. Yang, J. H. *et al.* Enhanced p-type dopability of P and As in CdTe using non-equilibrium thermal processing. *J. Appl. Phys.* **118**, 25102 (2015).
80. Wei, S.-H. & Zhang, S. B. Chemical trends of defect formation and doping limit in II-VI semiconductors: The case of CdTe. *Phys. Rev. B* **66**, 155211 (2002).
81. Barnard, E. S. *et al.* 3D Lifetime Tomography Reveals How CdCl<sub>2</sub> Improves Recombination Throughout CdTe Solar Cells. *Adv. Mater.* **29**, 1603801 (2017).
82. Moravec, P., Hage-Ali, M., Chibani, L. & Siffert, P. Deep levels in semi-insulating CdTe. *Mater. Sci. Eng. B* **16**, 223–227 (1993).
83. Balcioglu, A., Ahrenkiel, R. K. & Hasoon, F. Deep-level impurities in CdTe/CdS thin-film solar cells. *J. Appl. Phys.* **88**, 7175–7178 (2000).
84. Mathew, X. Photo-induced current transient spectroscopic study of the traps in CdTe. *Sol. Energy Mater. Sol. Cells* **76**, 225–242 (2003).
85. Komin, V. *et al.* The effect of the CdCl<sub>2</sub> treatment on CdTe/CdS thin film solar cells studied using deep level transient spectroscopy. *Thin Solid Films* **431–432**, 143–147 (2003).
86. Elhadidy, H., Franc, J., Moravec, P., Höschl, P. & Fiederle, M. Deep level defects in CdTe materials studied by thermoelectric effect spectroscopy and photoinduced current transient spectroscopy. *Semicond. Sci. Technol. Semicond. Sci. Technol* **22**, 537542 (2007).
87. Castaldini, A., Cavallini, A., Fraboni, B., Fernandez, P. & Piqueras, J. Deep energy levels in CdTe and CdZnTe. *J. Appl. Phys.* **83**, 2121–2126 (1998).
88. Kuciauskas, D. *et al.* Charge-carrier transport and recombination in heteroepitaxial CdTe. *J. Appl. Phys.* **116**, 123108 (2014).
89. Li, C. *et al.* Grain-Boundary-Enhanced Carrier Collection in CdTe Solar Cells. *Phys. Rev. Lett.* **112**, 156103 (2014).
90. Park, J. S., Yang, J. H., Barnes, T. & Wei, S. H. Effect of intermixing at CdS/CdTe interface on defect properties. *Appl. Phys. Lett.* **109**, 14–18 (2016).
91. Moseley, J. *et al.* Recombination by grain-boundary type in CdTe. *J. Appl. Phys.* **118**, (2015).
92. Visoly-Fisher, I., Cohen, S. R., Ruzin, A. & Cahen, D. How polycrystalline devices can outperform single-crystal ones: Thin film CdTe/CdS solar cells. *Adv. Mater.* **16**, 879–883 (2004).

93. Visoly-Fisher, I., Cohen, S. R., Gartsman, K., Ruzin, A. & Cahen, D. Understanding the beneficial role of grain boundaries in polycrystalline solar cells from single-grain-boundary scanning probe microscopy. *Adv. Funct. Mater.* **16**, 649–660 (2006).
94. Major, J. D. Grain boundaries in CdTe thin film solar cells: a review. *Semicond. Sci. Technol.* **31**, 93001 (2016).
95. Yan, Y., Al-Jassim, M. M. & Jones, K. M. Structure and effects of double-positioning twin boundaries in CdTe. *J. Appl. Phys.* **94**, 2976–2979 (2003).
96. Zhang, L. *et al.* Effect of Copassivation of Cl and Cu on CdTe Grain Boundaries. *Phys. Rev. Lett.* **101**, 155501 (2008).
97. Yang, J.-H., Shi, L., Wang, L.-W. & Wei, S.-H. Non-Radiative Carrier Recombination Enhanced by Two-Level Process: A First-Principles Study. *Sci. Rep.* **6**, 21712 (2016).
98. Durose, K., Edwards, P. R. & Halliday, D. P. Materials aspects of CdTe/CdS solar cells. *J. Cryst. Growth* **197**, 733–742 (1999).
99. Dharmadasa, I. Review of the CdCl<sub>2</sub> Treatment Used in CdS/CdTe Thin Film Solar Cell Development and New Evidence towards Improved Understanding. *Coatings* **4**, 282–307 (2014).
100. Yoo, S. *et al.* Identification of critical stacking faults in thin-film CdTe solar cells. *Appl. Phys. Lett.* **105**, 62104 (2014).
101. Kranz, L. *et al.* Tailoring Impurity Distribution in Polycrystalline CdTe Solar Cells for Enhanced Minority Carrier Lifetime. *Adv. Energy Mater.* **4**, 1301400 (2014).
102. Jensen, S. A. *et al.* Long carrier lifetimes in large-grain polycrystalline CdTe without CdCl<sub>2</sub>. *Appl. Phys. Lett.* **108**, 263903 (2016).
103. Ringel, S. A., Smith, A. W., MacDougall, M. H. & Rohatgi, A. The effects of CdCl<sub>2</sub> on the electronic properties of molecular-beam epitaxially grown CdTe/CdS heterojunction solar cells. *J. Appl. Phys.* **70**, 881–889 (1991).
104. Moutinho, H. R., Al-Jassim, M. M., Levi, D. H., Dippo, P. C. & Kazmerski, L. L. Effects of CdCl<sub>2</sub> treatment on the recrystallization and electro-optical properties of CdTe thin films. *J. Vac. Sci. Technol. A Vacuum, Surfaces, Film.* **16**, 1251–1257 (1998).
105. Abbas, A. *et al.* The effect of cadmium chloride treatment on close-spaced sublimated cadmium telluride thin-film solar cells. *IEEE J. Photovoltaics* **3**, 1361–1366 (2013).
106. McCandless, B. E., Moulton, L. V. & Birkmire, R. W. Recrystallization and sulfur diffusion in CdCl<sub>2</sub>-treated CdTe/CdS thin films. *Prog. Photovoltaics Res. Appl.* **5**, 249–260 (1997).
107. Metzger, W. K., Albin, D., Romero, M. J., Dippo, P. & Young, M. CdCl<sub>2</sub> treatment, S diffusion, and recombination in polycrystalline CdTe. *J. Appl. Phys.* **99**, 103703 (2006).
108. Williams, B. L. *et al.* A Comparative Study of the Effects of Nontoxic Chloride Treatments on CdTe Solar Cell Microstructure and Stoichiometry. *Adv. Energy Mater.* **5**, 1500554 (2015).
109. Major, J. D., Treharne, R. E., Phillips, L. J. & Durose, K. A low-cost non-toxic post-growth activation step for CdTe solar cells. *Nature* **511**, 334–337 (2014).
110. Jaffe, J. E. & Zunger, A. Electronic structure of the ternary chalcopyrite semiconductors CuAlS<sub>2</sub>, CuGaS<sub>2</sub>, CuInS<sub>2</sub>, CuAlSe<sub>2</sub>, CuGaSe<sub>2</sub>, and CuInSe<sub>2</sub>. *Phys. Rev. B* **28**, 5822–5847 (1983).
111. Butler, D. Thin films: ready for their close-up? *Nature* **454**, 558–559 (2008).
112. Noufi, R., Axton, R., Herrington, C. & Deb, S. K. Electronic properties versus composition of thin films of CuInSe<sub>2</sub>. *Appl. Phys. Lett.* **45**, 668–670 (1984).
113. Wei, S.-H., Zhang, S. B. & Zunger, A. Effects of Ga addition to CuInSe<sub>2</sub> on its electronic, structural, and defect properties. *Appl. Phys. Lett.* **72**, 3199–3201 (1998).
114. Zhang, S. B., Wei, S.-H., Zunger, A. & Katayama-Yoshida, H. Defect physics of the CuInSe<sub>2</sub> chalcopyrite

- semiconductor. *Phys. Rev. B* **57**, 9642 (1998).
115. Stephan, C., Schorr, S., Tovar, M. & Schock, H.-W. Comprehensive insights into point defect and defect cluster formation in CuInSe<sub>2</sub>. *Appl. Phys. Lett.* **98**, 91906 (2011).
  116. Malitckaya, M., Komsa, H. P., Havu, V. & Puska, M. J. First-Principles Modeling of Point Defects and Complexes in Thin-Film Solar-Cell Absorber CuInSe<sub>2</sub>. *Adv. Electron. Mater.* **3**, 1600353 (2017).
  117. Pohl, J. & Albe, K. Intrinsic point defects in CuInSe<sub>2</sub> and CuGaSe<sub>2</sub> as seen via screened-exchange hybrid density functional theory. *Phys. Rev. B* **87**, 245203 (2013).
  118. Fearheiley, M. L. The phase relations in the Cu,In,Se system and the growth of CuInSe<sub>2</sub> single crystals. *Sol. Cells* **16**, 91–100 (1986).
  119. Han, S.-H., Hasoon, F. S., Al-Thani, H. A., Hermann, A. M. & Levi, D. H. Effect of Cu deficiency on the defect levels of Cu<sub>0.86</sub>In<sub>1.09</sub>Se<sub>2.05</sub> determined by spectroscopic ellipsometry. *Appl. Phys. Lett.* **86**, 21903 (2005).
  120. Schmid, D., Ruckh, M., Grunwald, F. & Schock, H. W. Chalcopyrite/defect chalcopyrite heterojunctions on the basis of CuInSe<sub>2</sub>. *J. Appl. Phys.* **73**, 2902–2909 (1993).
  121. Ruberto, M. N. & Rothwarf, A. Time-dependent open-circuit voltage in CuInSe<sub>2</sub>/CdS solar cells: Theory and experiment. *J. Appl. Phys.* **61**, 4662–4669 (1987).
  122. Rau, U., Schmitt, M., Parisi, J., Riedl, W. & Karg, F. Persistent photoconductivity in Cu(In,Ga)Se<sub>2</sub> heterojunctions and thin films prepared by sequential deposition. *Appl. Phys. Lett.* **73**, 223–225 (1998).
  123. Heath, J. T., Cohen, J. D. & Shafarman, W. N. Bulk and metastable defects in CuIn<sub>1-x</sub>Ga<sub>x</sub>Se<sub>2</sub> thin films using drive-level capacitance profiling. *J. Appl. Phys.* **95**, 1000–1010 (2004).
  124. Harvey, S. P., Johnston, S. & Teeter, G. Effects of voltage-bias annealing on metastable defect populations in CIGS and CZTSe solar cells. in *2016 IEEE 43rd Photovoltaic Specialists Conference (PVSC) 2016–Novem*, 2169–2173 (IEEE, 2016).
  125. Teeter, G., Harvey, S. P. & Johnston, S. Controlling metastable native point-defect populations in Cu(In,Ga)Se<sub>2</sub> and Cu<sub>2</sub>ZnSnSe<sub>4</sub> materials and solar cells through voltage-bias annealing. *J. Appl. Phys.* **121**, 43102 (2017).
  126. Zabierowski, P., Rau, U. & Igalson, M. Classification of metastabilities in the electrical characteristics of ZnO/CdS/Cu(In,Ga)Se<sub>2</sub> solar cells. *Thin Solid Films* **387**, 147–150 (2001).
  127. Lany, S. & Zunger, A. Light- and bias-induced metastabilities in Cu(In,Ga)Se<sub>2</sub> based solar cells caused by the (V<sub>Se</sub>-V<sub>Cu</sub>) vacancy complex. *J. Appl. Phys.* **100**, 113715–113725 (2006).
  128. Lang, D. V. & Logan, R. A. Large-Lattice-Relaxation Model for Persistent Photoconductivity in Compound Semiconductors. *Phys. Rev. Lett.* **39**, 635–639 (1977).
  129. Chadi, D. J. & Chang, K. J. Theory of the Atomic and Electronic Structure of DX Centers in GaAs and Al<sub>x</sub>Ga<sub>1-x</sub>As Alloys. *Phys. Rev. Lett.* **61**, 873–876 (1988).
  130. Thio, T., Bennett, J. W., Chadi, D. J., Linke, R. A. & Tamargo, M. C. DX centers in II-VI semiconductors and heterojunctions. *J. Electron. Mater.* **25**, 229–233 (1996).
  131. Lany, S. & Zunger, A. Intrinsic DX Centers in Ternary Chalcopyrite Semiconductors. *Phys. Rev. Lett.* **100**, 16401 (2008).
  132. Niles, D. W. *et al.* Na impurity chemistry in photovoltaic CIGS thin films: Investigation with x-ray photoelectron spectroscopy. *J. Vac. Sci. Technol. A Vacuum, Surfaces, Film.* **15**, 3044–3049 (1997).
  133. Kimura, R. *et al.* Effects of Sodium on CuIn<sub>3</sub>Se<sub>5</sub> Thin Films. *Jpn. J. Appl. Phys.* **38**, L899–L901 (1999).
  134. Pianezzi, F. *et al.* Unveiling the effects of post-deposition treatment with different alkaline elements on the electronic properties of CIGS thin film solar cells. *Phys. Chem. Chem. Phys.* **16**, 8843 (2014).
  135. Lammer, M., Klemm, U. & Powalla, M. Sodium co-evaporation for low temperature Cu(In,Ga)Se<sub>2</sub> deposition. *Thin Solid Films* **387**, 33–36 (2001).

136. Wei, S.-H., Zhang, S. B. & Zunger, A. Effects of Na on the electrical and structural properties of CuInSe<sub>2</sub>. *J. Appl. Phys.* **85**, 7214–7218 (1999).
137. Oikkonen, L. E., Ganchenkova, M. G., Seitsonen, A. P. & Nieminen, R. M. Effect of sodium incorporation into CuInSe<sub>2</sub> from first principles. *J. Appl. Phys.* **114**, 83503 (2013).
138. Yuan, Z. K. *et al.* Na-Diffusion Enhanced p-type Conductivity in Cu(In,Ga)Se<sub>2</sub>: A New Mechanism for Efficient Doping in Semiconductors. *Adv. Energy Mater.* **6**, 1–7 (2016).
139. Forest, R. V., Eser, E., McCandless, B. E., Chen, J. G. & Birkmire, R. W. Reversibility of (Ag,Cu)(In,Ga)Se<sub>2</sub> electrical properties with the addition and removal of Na: Role of grain boundaries. *J. Appl. Phys.* **117**, 115102 (2015).
140. Kronik, L., Cahen, D. & Schock, H. W. Effects of Sodium on Polycrystalline Cu(In,Ga)Se<sub>2</sub> and Its Solar Cell Performance. *Adv. Mater.* **10**, 31–36 (1998).
141. Persson, C. & Zunger, A. Anomalous Grain Boundary Physics in Polycrystalline CuInSe<sub>2</sub>: The Existence of a Hole Barrier. *Phys. Rev. Lett.* **91**, 266401 (2003).
142. Siebentritt, S., Igalson, M., Persson, C. & Lany, S. The electronic structure of chalcopyrites - Bands, point defects and grain boundaries. *Prog. Photovoltaics Res. Appl.* **18**, 390–410 (2010).
143. Abou-Ras, D. *et al.* Direct insight into grain boundary reconstruction in polycrystalline Cu(In,Ga)Se<sub>2</sub> with atomic resolution. *Phys. Rev. Lett.* **108**, 75502 (2012).
144. Yin, W.-J., Wu, Y., Noufi, R., Al-Jassim, M. & Yan, Y. Defect segregation at grain boundary and its impact on photovoltaic performance of CuInSe<sub>2</sub>. *Appl. Phys. Lett.* **102**, 193905 (2013).
145. Keller, D. *et al.* Band gap widening at random CIGS grain boundary detected by valence electron energy loss spectroscopy. *Appl. Phys. Lett.* **109**, 153103 (2016).
146. Goodman, C. H. L. The prediction of semiconducting properties in inorganic compounds. *J. Phys. Chem. Solids* **6**, 305–314 (1958).
147. Pamplin, B. . A systematic method of deriving new semiconducting compounds by structural analogy. *J. Phys. Chem. Solids* **25**, 675–684 (1964).
148. Pamplin, B. R. & Shah, J. S. Studies in the Adamantine Family of Semiconductors. *J. Electrochem. Soc.* **116**, 1565 (1969).
149. Chen, S., Gong, X. G., Walsh, A. & Wei, S.-H. Electronic structure and stability of quaternary chalcogenide semiconductors derived from cation cross-substitution of II-VI and I-III-VI<sub>2</sub> compounds. *Phys. Rev. B* **79**, 165211 (2009).
150. Walsh, A., Chen, S., Wei, S.-H. & Gong, X.-G. Kesterite Thin-Film Solar Cells: Advances in Materials Modelling of Cu<sub>2</sub>ZnSnS<sub>4</sub>. *Adv. Energy Mater.* **2**, 400–409 (2012).
151. Chen, S. Y. *et al.* Compositional dependence of structural and electronic properties of Cu<sub>2</sub>ZnSn(S,Se)<sub>4</sub> alloys for thin film solar cells. *Phys. Rev. B* **83**, 125201 (2011).
152. Wallace, S. K., Mitzi, D. B. & Walsh, A. The Steady Rise of Kesterite Solar Cells. *ACS Energy Lett.* **2**, 776–779 (2017).
153. Wang, W. *et al.* Device Characteristics of CZTSSe Thin-Film Solar Cells with 12.6% Efficiency. *Adv. Energy Mater.* **4**, 1301465 (2014).
154. Bourdais, S. *et al.* Is the Cu/Zn disorder the main culprit for the voltage deficit in kesterite solar cells? *Adv. Energy Mater.* **6**, 1502276 (2016).
155. Chen, S., Walsh, A., Gong, X.-G. & Wei, S.-H. Classification of Lattice Defects in the Kesterite Cu<sub>2</sub>ZnSnS<sub>4</sub> and Cu<sub>2</sub>ZnSnSe<sub>4</sub> Earth-Abundant Solar Cell Absorbers. *Adv. Mater.* **25**, 1522–1539 (2013).
156. Chen, S. Y., Yang, J.-H. H., Gong, X. G., Walsh, A. & Wei, S.-H. H. Intrinsic point defects and complexes in the quaternary kesterite semiconductor Cu<sub>2</sub>ZnSnS<sub>4</sub>. *Phys. Rev. B* **81**, 245204 (2010).
157. Chen, S., Gong, X. G., Walsh, A. & Wei, S.-H. H. Defect physics of the kesterite thin-film solar cell absorber

- Cu<sub>2</sub>ZnSnS<sub>4</sub>. *Appl. Phys. Lett.* **96**, 21902 (2010).
158. Yoo, H. & Fauchet, P. Dielectric constant reduction in silicon nanostructures. *Phys. Rev. B* **77**, 115355 (2008).
  159. Han, D. *et al.* Deep electron traps and origin of p-type conductivity in the earth-abundant solar-cell material Cu<sub>2</sub>ZnSnS<sub>4</sub>. *Phys. Rev. B* **87**, 155206 (2013).
  160. Zhai, Y. T. *et al.* Structural diversity and electronic properties of Cu<sub>2</sub>SnX<sub>3</sub> (X = S, Se): A first-principles investigation. *Phys. Rev. B* **84**, 75213 (2011).
  161. Burton, L. A., Kumagai, Y., Walsh, A. & Oba, F. DFT investigation into the underperformance of sulfide materials in photovoltaic applications. *J. Mater. Chem. A* **5**, 9132–9140 (2017).
  162. Schorr, S. The crystal structure of kesterite type compounds: A neutron and X-ray diffraction study. *Sol. Energy Mater. Sol. Cells* **95**, 1482–1488 (2011).
  163. Paris, M., Choubrac, L., Lafond, A., Guillot-Deudon, C. & Jobic, S. Solid-State NMR and Raman Spectroscopy To Address the Local Structure of Defects and the Tricky Issue of the Cu/Zn Disorder in Cu-Poor, Zn-Rich CZTS Materials. *Inorg. Chem.* **53**, 8646–8653 (2014).
  164. Dimitrievska, M., Fairbrother, A., Saucedo, E., Pérez-Rodríguez, A. & Izquierdo-Roca, V. Influence of compositionally induced defects on the vibrational properties of device grade Cu<sub>2</sub>ZnSnSe<sub>4</sub> absorbers for kesterite based solar cells. *Appl. Phys. Lett.* **106**, 73903 (2015).
  165. Schorr, S. Structural aspects of adamantite like multinary chalcogenides. *Thin Solid Films* **515**, 5985–5991 (2007).
  166. Choubrac, L. *et al.* Multinuclear (<sup>67</sup>Zn, <sup>119</sup>Sn and <sup>65</sup>Cu) NMR spectroscopy – an ideal technique to probe the cationic ordering in Cu<sub>2</sub>ZnSnS<sub>4</sub> photovoltaic materials. *Phys. Chem. Chem. Phys.* **15**, 10722 (2013).
  167. Scragg, J. J. S., Choubrac, L., Lafond, A., Ericson, T. & Platzer-Björkman, C. A low-temperature order-disorder transition in Cu<sub>2</sub>ZnSnS<sub>4</sub> thin films. *Appl. Phys. Lett.* **104**, 41911 (2014).
  168. Rey, G. *et al.* The band gap of Cu<sub>2</sub>ZnSnSe<sub>4</sub>: Effect of order-disorder. *Appl. Phys. Lett.* **105**, 112106 (2014).
  169. Valentini, M. *et al.* Effect of the order-disorder transition on the optical properties of Cu<sub>2</sub>ZnSnS<sub>4</sub>. *Appl. Phys. Lett.* **108**, 211909 (2016).
  170. Rudisch, K., Ren, Y., Platzer-Björkman, C. & Scragg, J. Order-disorder transition in B-type Cu<sub>2</sub>ZnSnS<sub>4</sub> and limitations of ordering through thermal treatments. *Appl. Phys. Lett.* **108**, 231902 (2016).
  171. Scragg, J. J. S. *et al.* Cu-Zn Disorder and Band Gap Fluctuations in Cu<sub>2</sub>ZnSn(S,Se)<sub>4</sub>: Theoretical and Experimental Investigations. *Phys. Status Solidi* **253**, 247–254 (2016).
  172. Zawadzki, P., Zakutayev, A. & Lany, S. Entropy-Driven Clustering in Tetrahedrally Bonded Multinary Materials. *Phys. Rev. Appl.* **3**, 1–7 (2015).
  173. Repins, I. L. *et al.* Indications of short minority-carrier lifetime in kesterite solar cells. *J. Appl. Phys.* **114**, 1–5 (2013).
  174. Liu, F. *et al.* Nanoscale Microstructure and Chemistry of Cu<sub>2</sub>ZnSnS<sub>4</sub>/CdS Interface in Kesterite Cu<sub>2</sub>ZnSnS<sub>4</sub> Solar Cells. *Adv. Energy Mater.* **6**, 1600706 (2016).
  175. Hages, C. J. *et al.* Identifying the Real Minority Carrier Lifetime in Nonideal Semiconductors: A Case Study of Kesterite Materials. **116**, 1700110–1700167 (2017).
  176. Kim, S., Park, J.-S. & Walsh, A. Identification of Killer Defects in Kesterite Thin-Film Solar Cells. *ACS Energy Lett.* **3**, 496–500 (2018).
  177. Møller, C. K. Crystal Structure and Photoconductivity of Cæsium Plumbohalides. *Nature* **182**, 1436–1436 (1958).
  178. Weber, D. CH<sub>3</sub>NH<sub>3</sub>PbX<sub>3</sub>, a Pb(II)-System with Cubic Perovskite Structure. *Zeitschrift für Naturforsch. B* **33b**, 1443–1445 (1978).
  179. Kojima, A., Teshima, K., Shirai, Y. & Miyasaka, T. Organometal Halide Perovskites as Visible-light

- Sensitizers for Photovoltaic Cells. *J. Am. Chem. Soc.* **131**, 6050–6051 (2009).
180. Stranks, S. D. & Snaith, H. J. Metal-halide perovskites for photovoltaic and light-emitting devices. *Nat. Nanotechnol.* **10**, 391–402 (2015).
  181. Walsh, A. Principles of Chemical Bonding and Band Gap Engineering in Hybrid Organic–Inorganic Halide Perovskites. *J. Phys. Chem. C* **119**, 5755–5760 (2015).
  182. Brivio, F., Butler, K. T., Walsh, A. & Van Schilfgaarde, M. Relativistic quasiparticle self-consistent electronic structure of hybrid halide perovskite photovoltaic absorbers. *Phys. Rev. B* **89**, 155204 (2014).
  183. Frost, J. M. & Walsh, A. What Is Moving in Hybrid Halide Perovskite Solar Cells? *Acc. Chem. Res.* **49**, 528–535 (2016).
  184. Yin, W.-J., Shi, T. & Yan, Y. Unusual defect physics in CH<sub>3</sub>NH<sub>3</sub>PbI<sub>3</sub> perovskite solar cell absorber. *Appl. Phys. Lett.* **104**, 63903 (2014).
  185. Brandt, R. E., Stevanović, V., Ginley, D. S. & Buonassisi, T. Identifying defect-tolerant semiconductors with high minority-carrier lifetimes: beyond hybrid lead halide perovskites. *MRS Commun.* **5**, 265 (2015).
  186. Walsh, A. & Zunger, A. Instilling defect tolerance in new compounds. *Nat. Mater.* **16**, 964–967 (2017).
  187. Stoddard, R. J., Eickemeyer, F. T., Katahara, J. K. & Hillhouse, H. W. Correlation between Photoluminescence and Carrier Transport and a Simple In Situ Passivation Method for High-Bandgap Hybrid Perovskites. *J. Phys. Chem. Lett.* **8**, 3289–3298 (2017).
  188. Onoda-Yamamuro, N., Matsuo, T. & Suga, H. Dielectric Study of CH<sub>3</sub>NH<sub>3</sub>PbX<sub>3</sub> (X = Cl, Br, I). *J. Phys. Chem. Solids* **53**, 935–939 (1992).
  189. Baumann, A. *et al.* Identification of Trap States in Perovskite Solar Cells. *J. Phys. Chem. Lett.* **6**, 2350–2354 (2015).
  190. Yang, W. S. *et al.* Iodide management in formamidinium-lead-halide-based perovskite layers for efficient solar cells. *Science* **356**, 1376–1379 (2017).
  191. Eames, C. *et al.* Ionic transport in hybrid lead iodide perovskite solar cells. *Nat. Commun.* **6**, 7497 (2015).
  192. Kim, G. Y. *et al.* Large tunable photoeffect on ion conduction in halide perovskites and implications for photodecomposition. *Nat. Mater.* **2018** 1 (2018). doi:10.1038/s41563-018-0038-0
  193. Umari, P., Mosconi, E. & De Angelis, F. Relativistic GW calculations on CH<sub>3</sub>NH<sub>3</sub>PbI<sub>3</sub> and CH<sub>3</sub>NH<sub>3</sub>SnI<sub>3</sub> perovskites for solar cell applications. *Sci. Rep.* **4**, 4467 (2014).
  194. Du, M.-H. Density Functional Calculations of Native Defects in CH<sub>3</sub>NH<sub>3</sub>PbI<sub>3</sub>: Effects of Spin–Orbit Coupling and Self-Interaction Error. *J. Phys. Chem. Lett.* **6**, 1461–1466 (2015).
  195. Walsh, A., Scanlon, D. O., Chen, S., Gong, X. G. & Wei, S.-H. Self-regulation mechanism for charged point defects in hybrid-halide perovskites. *Angew. Chemie Int. Ed.* **54**, 1791–1794 (2015).
  196. Mandel, G. Self-compensation limited conductivity in binary semiconductors. I. Theory. *Phys. Rev.* **134**, A1073 (1964).
  197. Whalley, L. D., Crespo-Otero, R. & Walsh, A. H-Center and V-Center Defects in Hybrid Halide Perovskites. *ACS Energy Lett.* **2**, 2713–2714 (2017).
  198. Tasker, P. W. & Stoneham, A. M. An Appraisal of the Molecular Model for the F<sub>2</sub> centre. *J. Phys. Chem. Solids* **38**, 1185–1189 (1977).
  199. Shluger, A. L., Puchin, V. E., Suzuki, T., Tanimura, K. & Itoh, N. Optical transitions of the H centers in alkali halides. *Phys. Rev. B* **52**, 4017–4028 (1995).
  200. Zohar, A. *et al.* What Is the Mechanism of MAPbI<sub>3</sub> p-Doping by I<sub>2</sub>? Insights from Optoelectronic Properties. *ACS Energy Lett.* **2**, 2408–2414 (2017).
  201. Article, E. *et al.* Reversible photo-induced trap formation in mixed-halide hybrid perovskites for photovoltaics. *Chem. Sci.* **6**, 613–617 (2015).



202. Mosconi, E. *et al.* Light-induced annihilation of Frenkel defects in organo-lead halide perovskites. *Energy Environ. Sci.* **9**, 3180–3187 (2016).
203. Grancini, G. *et al.* Role of microstructure in the electron–hole interaction of hybrid lead halide perovskites. *Nat. Photonics* **9**, 695–702 (2015).
204. Yang, T.-Y., Gregori, G., Pellet, N., Grätzel, M. & Maier, J. Significance of ion conduction in a organic-inorganic lead-iodide-based perovskite photosensitizer. *Angew. Chemie Int. Ed.* **54**, 7905–7910 (2015).
205. Zakutayev, A., Perry, N. H., Mason, T. O., Ginley, D. S. & Lany, S. Non-equilibrium origin of high electrical conductivity in gallium zinc oxide thin films. *Appl. Phys. Lett.* **103**, 232106 (2013).
206. Zhang, S. B., Wei, S.-H. & Zunger, A. Microscopic Origin of the Phenomenological Equilibrium ‘Doping Limit Rule’ in n-Type III-V Semiconductors. *Phys. Rev. Lett.* **84**, 1232 (2000).
207. Walukiewicz, W. Mechanism of Fermi-level stabilization in semiconductors. *Phys. Rev. B* **37**, 4760 (1988).
208. Zunger, A. Practical doping principles. *Appl. Phys. Lett.* **83**, 57–59 (2003).
209. Wei, S.-H. Overcoming the doping bottleneck in semiconductors. *Comput. Mater. Sci.* **30**, 337–348 (2004).
210. Zhang, S. B., Wei, S.-H. & Zunger, A. A phenomenological model for systematization and prediction of doping limits in II–VI and I–III–V<sub>2</sub> compounds. *J. Appl. Phys.* **83**, 3192 (1998).
211. Walsh, A. *et al.* Limits to Doping of Wide Band Gap Semiconductors. *Chem. Mater.* **25**, 2924 (2013).
212. Buckeridge, J. *et al.* Polymorph Engineering of TiO<sub>2</sub>: Demonstrating How Absolute Reference Potentials Are Determined by Local Coordination. *Chem. Mater.* **27**, 3844–3851 (2015).
213. Shi, L. & Wang, L.-W. Ab initio Calculations of Deep-Level Carrier Nonradiative Recombination Rates in Bulk Semiconductors. *Phys. Rev. Lett.* **109**, 245501 (2012).
214. Alkauskas, A., Yan, Q., de Walle, C. G. & Van De Walle, C. G. First-principles theory of nonradiative carrier capture via multiphonon emission. *Phys. Rev. B* **90**, 17–27 (2014).
215. Mandelkorn, J. & Lamneck, J. H. Simplified fabrication of back surface electric field silicon cells and novel characteristics of such cells. *Sol. Cells* **29**, 121–130 (1990).
216. Lundberg, O., Bodegård, M., Malmström, J. & Stolt, L. Influence of the Cu(In,Ga)Se<sub>2</sub> thickness and Ga grading on solar cell performance. *Prog. Photovoltaics Res. Appl.* **11**, 77–88 (2003).
217. Lee, M., Ngan, L., Hayes, W., Sorensen, J. & Panchula, A. F. Understanding next generation cadmium telluride photovoltaic performance due to spectrum. in *2015 IEEE 42nd Photovoltaic Specialist Conference (PVSC)* 1–6 (IEEE, 2015). doi:10.1109/PVSC.2015.7356003
218. Sinsermsuksakul, P. *et al.* Overcoming Efficiency Limitations of SnS-Based Solar Cells. *Adv. Energy Mater.* **4**, 1400496 (2014).
219. Polizzotti, A. *et al.* Improving the Carrier Lifetime of Tin Sulfide via Prediction and Mitigation of Harmful Point Defects. *J. Phys. Chem. Lett.* **8**, 3661–3667 (2017).
220. Shockley, W. & Queisser, H. J. Detailed balance limit of efficiency of p-n junction solar cells. *J. Appl. Phys.* **32**, 510–519 (1961).
221. Yu, L. & Zunger, A. Identification of Potential Photovoltaic Absorbers Based on First-Principles Spectroscopic Screening of Materials. *Phys. Rev. Lett.* **108**, 68701 (2012).
222. Blank, B., Kirchartz, T., Lany, S. & Rau, U. Selection Metric for Photovoltaic Materials Screening Based on Detailed-Balance Analysis. *Phys. Rev. Appl.* **8**, 24032 (2017).
223. Steirer, K. X. *et al.* Defect Tolerance in Methylammonium Lead Triiodide Perovskite. *ACS Energy Lett.* **1**, 360–366 (2016).
224. Zakutayev, A. *et al.* Defect tolerant semiconductors for solar energy conversion. *Journal of Physical Chemistry Letters* **5**, 1117–1125 (2014).
225. Hendon, C. H. *et al.* Electroactive Nanoporous Metal Oxides and Chalcogenides by Chemical Design. *Chem.*

- Mater.* **29**, 3663–3670 (2017).
226. Ganose, A. M., Savory, C. N. & Scanlon, D. O. Beyond methylammonium lead iodide: prospects for the emergent field of ns<sup>2</sup> containing solar absorbers. *Chem. Commun.* **103**, 15729–15735 (2016).
  227. Tan, Y. P., Povolotskyi, M., Kubis, T., Boykin, T. B. & Klimeck, G. Tight-binding analysis of Si and GaAs ultrathin bodies with subatomic wave-function resolution. *Phys. Rev. B* **92**, 85301 (2015).
  228. Menéndez-Proupin, E., Amézaga, A. & Cruz Hernández, N. Electronic structure of CdTe using GGA+USIC. *Phys. B Condens. Matter* **452**, 119–123 (2014).
  229. Park, J. S., Yang, J. H., Ramanathan, K. & Wei, S. H. Defect properties of Sb- and Bi-doped CuInSe<sub>2</sub>: The effect of the deep lone-pair s states. *Appl. Phys. Lett.* **105**, 243901 (2014).
  230. Brivio, F., Butler, K. T. K. T., Walsh, A. & Van Schilfgaarde, M. Relativistic Quasiparticle Self-consistent Electronic Structure of Hybrid Halide Perovskite Photovoltaic Absorbers. *Phys. Rev. B* **89**, 155204 (2014).
  231. Redinger, A. *et al.* Time resolved photoluminescence on Cu(In, Ga)Se<sub>2</sub> absorbers: Distinguishing degradation and trap states. *Appl. Phys. Lett.* **110**, 122104 (2017).
  232. Stranks, S. D. *et al.* Electron-Hole Diffusion Lengths Exceeding 1 Micrometer in an Organometal Trihalide Perovskite Absorber. *Science* **342**, 341–344 (2013).
  233. Yang, Y. *et al.* Comparison of Recombination Dynamics in CH<sub>3</sub>NH<sub>3</sub>PbBr<sub>3</sub> and CH<sub>3</sub>NH<sub>3</sub>PbI<sub>3</sub> Perovskite Films: Influence of Exciton Binding Energy. *J. Phys. Chem. Lett.* **6**, 4688–4692 (2015).
  234. Shi, D. *et al.* Low trap-state density and long carrier diffusion in organolead trihalide perovskite single crystals. *Science* **347**, 519–522 (2015).
  235. deQuilettes, D. W. *et al.* Photoluminescence Lifetimes Exceeding 8  $\mu$ s and Quantum Yields Exceeding 30% in Hybrid Perovskite Thin Films by Ligand Passivation. *ACS Energy Lett.* **1**, 438–444 (2016).
  236. Poindexter, E. H. *et al.* Electronic traps and Pb centers at the Si/SiO<sub>2</sub> interface: Band-gap energy distribution. *J. Appl. Phys.* **56**, 2844–2849 (1984).
  237. Huang, B. *et al.* Origin of reduced efficiency in Cu(In,Ga)Se<sub>2</sub> solar cells with high Ga concentration: Alloy solubility versus intrinsic defects. *IEEE J. Photovoltaics* **4**, 477–482 (2014).
  238. Krysztopa, A., Igalson, M., Gütay, L., Larsen, J. K. & Aida, Y. Defect level signatures in CuInSe<sub>2</sub> by photocurrent and capacitance spectroscopy. *Thin Solid Films* **535**, 366–370 (2013).